December 2002 • NREL/SR-520-33164

Subcontractor Report

Electroabsorption and Transport Measurements and Modeling Research in Amorphous Silicon Based Solar Cells

Final Technical Report
24 March 1998—15 August 2002

E.A. Schiff, A.R. Middya, J. Lyou, N. Kopidakis, S. Rane, P. Rao, Q. Yuan, and K. Zhu
Syracuse University
Syracuse, New York

National Renewable Energy Laboratory

1617 Cole Boulevard
Golden, Colorado 80401-3393

NREL is a U.S. Department of Energy Laboratory
Operated by Midwest Research Institute • Battelle • Bechtel

Contract No. DE-AC36-99-GO10337

December 2002 • NREL/SR-520-33164

Electroabsorption and Transport Measurements and Modeling Research in Amorphous Silicon Based Solar Cells

Final Technical Report
24 March 1998—15 August 2002

E.A. Schiff, A.R. Middya, J. Lyou, N. Kopidakis, S. Rane, P. Rao, Q. Yuan, and K. Zhu
Syracuse University
Syracuse, New York

NREL Technical Monitor: B. von Roedern

Prepared under Subcontract No. XAK-8-17619-23

National Renewable Energy Laboratory

1617 Cole Boulevard
Golden, Colorado 80401-3393

NREL is a U.S. Department of Energy Laboratory
Operated by Midwest Research Institute • Battelle • Bechtel

Contract No. DE-AC36-99-GO10337

NOTICE

Available electronically at http://www.osti.gov/bridge

Available for a processing fee to U.S. Department of Energy
and its contractors, in paper, from:

U.S. Department of Energy
Office of Scientific and Technical Information
P.O. Box 62
Oak Ridge, TN 37831-0062
phone: 865.576.8401
fax: 865.576.5728
email: reports@adonis.osti.gov

Available for sale to the public, in paper, from:

U.S. Department of Commerce
National Technical Information Service
5285 Port Royal Road
Springfield, VA 22161
phone: 800.553.6847
fax: 703.605.6900
email: orders@ntis.fedworld.gov
online ordering: http://www.ntis.gov/ordering.htm

Printed on paper containing at least 50% wastepaper, including 20% postconsumer waste

Introduction

Preface

The contributions of this research project to amorphous silicon solar cells are in the following areas:

- *Improved understanding of the open-circuit voltage*. We have developed a "thermionic emission model" which explains how defective interfaces in a-Si:H *pin* cells cause diminished values of V_{OC}.
- *Improved knowledge of the built-in potential.* Our estimates of V_{BI} are about 1.2 V in a-SiGe cells. V_{BI} is crucial to understanding the performance of a-Si:H solar cells.
- *Variations in hole drift-mobilities for differing forms of a-Si:H*. We found that both hot-wire deposited a-Si:H and also hydrogen-dilution during plasma deposition yield larger hole drift-mobilities.
- *Infrared spectroscopy of interfaces in a-Si:H cells.* We discovered a method which yields the spectrum of the *p/i* and *n/i* interfaces in a-Si:H solar cells. We made progress in understanding these spectra, although much remains to be done.
- *Polymer p-layers*. We explored a hole conducting polymer (PEDT:PSS) as the *p*-layer in a-Si:H *pin* cells; the open-circuit voltage is about 0.7 V.
- *Hydrogen based models for defects & metastability*. We showed how how previous work on hydrogen and defects in a-Si:H relates to the more recent "hydrogen collision" model for the Staebler-Wronski effect.

Summary

Improved understanding of the open-circuit voltage. The measured magnitude of the open-circuit voltage V_{OC} has never been conclusively explained in terms of fundamental measurements, and there thus remains some possibility that a significant increase can be achieved. In this project we found using electroabsorption measurements that the built-in potential drops across the bulk of the intrinsic layer in a-Si and a-SiGe *pin* cells are about 1.2 V. This value was integrated into computer modeling studies, which led to a "thermionic emission" model for understanding the influence of *p* and *n* layers upon V_{OC}. However, we did not achieve a conclusive understanding of V_{OC} values during this project. Based on subsequent work, we believe that the best values of V_{OC} are *not* presently limited by doped layers; further improvements in V_{OC} may be achievable if the hole drift mobility can be improved.

Variations in hole drift-mobilities for differing forms of a-Si:H. Until fairly recently, the drift mobility of holes appeared to be fairly constant for a-Si materials varying in bandgap (via Ge and C alloying) and defect density. This relative constancy is most likely the reason that the best values for V_{OC} vary 1:1 with the bandgap. Since the work by Ganguly on triode-deposited a-Si:H, the possibility of sizable variations in the hole drift mobility has been viewed more seriously. In this project we found that a-Si:H materials made under conditions of hydrogen dilution show a significant improvement in hole drift mobility. We believe that this improvement most likely leads to an increase in V_{OC} beyond that which can be explained simply by the increase in bandgap, but this speculation has not been proven.

Infrared spectroscopy of interfaces in a-Si:H cells. There is no doubt that *p/i* interfaces significantly affect a-Si based solar cells. Both *in-situ* optical and electrons spectroscopies, as well as *ex situ* capacitance studies, have been used to explore the *p/i* and *n/i* interfaces. We discovered a new way to measure infrared spectra for these interfaces, and have used this to demonstrate the likelihood of doping

complexing in *n*-type a-Si. We have also explored the use of optical bias to isolate the *p/i* contribution to the spectrum.

Polymer p-layers. The ideal *p*-type window material for a-Si based solar cells would have a larger bandgap than the presently used materials (a-SiC:H and nc-Si:H). Hole transporting polymers could be an interesting alternative. We explored one such material (PEDT:PSS), and found V_{OC} of about 0.7 V. This result is not surprising, since this polymer's bandgap is not significantly wider than the present *p*-layers. Nonetheless the experiment indicates the validity of the basic device concept, and suggests that further studies with other polymers or organics may yield superior values.

Hydrogen based models for defects & metastability. The "hydrogen collision" model for the Staebler-Wronski effect recently proposed by Branz is an interesting explanation for light-soaking effects in a-Si:H. We showed how this model can be integrated with the "hydrogen deficit" model proposed some years ago by Zafar and Schiff to explain thermally generated metastabilities and hydrogen evolution effects.

Publications & Manuscripts Acknowledging Subcontract Support

"Photovoltaic Effect in Polymer-Amorphous Silicon Heterojunction Devices," A. R. Middya and E. A. Schiff, submitted.

"Infrared Modulation Spectroscopy of Interfaces in Amorphous Silicon Solar Cells," K. Zhu, E. A. Schiff, and G. Ganguly, *J. Non-Cryst. Solids* **299-302**, 1162-1166 (2002)..

"Electroabsorption Measurements and Built-in Potentials in Amorphous Silicon-Germanium Solar Cells," J. H. Lyou, E. A. Schiff, S. Guha, and J. Yang, *Appl. Phys. Lett.* **78**, 1924-1926 (2001).

"Open-Circuit Voltage Physics in Amorphous Silicon Solar Cells," L. Jiang, J. H. Lyou, S. Rane, E. A. Schiff, Q. Wang, and Q. Yuan, in *Amorphous and Heterogeneous Films – 2000*, edited by H. M. Branz, R. W. Collins, S. Guha, H. Okamoto, and M. Stutzmann (Materials Research Society, Symposium Proceedings Vol. 609, Pittsburgh, 2001), A18.3.1-12.

"Interfacial Optical Spectra in Amorphous Silicon Based pin Solar Cells," Kai Zhu, J. H. Lyou, E. A. Schiff, R. S. Crandall, G. Ganguly, S. S. Hegedus, in *Conference Record of the 28th IEEE Photovoltaics Specialists Conference* (Institute of Electrical and Electronics Engineers, Inc., Piscataway, 2000) 725-727.

"Charge Modulation Spectra in Phosphorus-Doped a-Si:H," J.-H. Lyou, N. Kopidakis, E. A. Schiff, *J. Non-Cryst. Solids* **266-269**, 227-231 (2000).

"Hydrogen-mediated models for metastability in a-Si:H: role of dihydride bonding," N. Kopidakis and E. A. Schiff, *J. Non-Cryst. Solids* **266-269**, 415-418 (2000).

"Infrared Electroabsorption Spectra in Amorphous Silicon Solar Cells," J. H. Lyou, E. A. Schiff, S. S. Hegedus, S. Guha, and J. Yang, in *Amorphous and Heterogeneous Silicon Thin Films: Fundamentals to Devices - 1999* (Materials Research Society, Symposium Proceedings Vol. 557, Pittsburgh, 1999), pp. 457-463.

"Grazing Incidence Measurements of Polarized Electroabsorption and Light Soaking Effect on Amorphous Silicon Based Solar Cells," L. Jiang, E. A. Schiff, Q. Wang, S. Guha, and J. Yang, in *Amorphous and Microcrytalline Silicon Technology - 1998*, edited by R. Schropp, H.M. Branz, M. Hack, I. Shimizu, and S. Wagner (Materials Research Society Symposium Proceedings Vol. 507, Pittsburgh, 1999), 631-636.

"Polarized Electroabsorption Spectra and Light Soaking of Solar Cells Based on Hydrogenated Amorphous Silicon," L. Jiang, Q. Wang, E. A. Schiff, S. Guha, and J. Yang, *Appl. Phys. Lett.* **72**, 1060-1062 (1998).

Acknowledgments

The work reported here includes contributions from many scientific collaborators, including:

- Homer Antoniadis (Osram Corporation)
- Dick Crandall (National Renewable Energy Laboratory)
- Kelly Douglas (Bayer Corporation)
- Gautam Ganguly (BP Solar)
- Subhendu Guha (United Solar Systems Corp.)
- Jill Simpson (Bayer Corporation)
- Qi Wang (National Renewable Energy Laboratory)
- Chris Wronski (Pennsylvania State University)
- Jeff Yang (United Solar Systems Corp.)

Table of Contents

Table of Figures

Electroabsorption measurements and built-in potentials

Introduction

The built-in potential V_{bi} across a solar cell is among its most important device parameters. For amorphous silicon-based solar cells, there is at best only a semi-quantitative knowledge of V_{bi}. The two most promising approaches for estimating V_{bi} are *electroabsorption* measurements [1], which infer V_{bi} from the dependence of optical absorption upon electric-field, and *low-temperature saturation* of the open-circuit voltage V_{oc}, which may be identifiable with V_{bi}.[2] Neither method has proved to be ideal in previous work. The interpretation of electroabsorption depends upon the distribution of the internal electric field between the intrinsic and p^+ layers of a cell, which greatly complicates estimation of V_{bi}. The low-temperature saturation method of course depends upon a particular assumption about the electrical properties of a cell at low temperatures which is also difficult to justify conclusively.

Most prior work on V_{bi} has emphasized amorphous-silicon solar cells with "standard" a-Si:H absorbers (optical gaps about 1.75 eV). In the present work we present electroabsorption measurements on cells with narrow bandgap absorbers based on a-SiGe:H alloys. This work is of course a potentially useful extension of the earlier measurements, since there is (to our knowledge) no experimental information on V_{bi} in cells incorporating a-SiGe. Perhaps equally important, our results indicate that electroabsorption measurements in solar cells with a-SiGe:H absorber layers largely avoid the interpretive difficulties associated with cells with a-Si:H absorbers. For the latter, the p^+ and intrinsic layers have comparable, but quantitatively different, electroabsorption spectra. This complicates estimation of V_{bi}. For cells with a-SiGe:H absorber layers, the electroabsorption signal is much more completely dominated by the behavior of the a-SiGe:H absorber layer, leading to a more direct estimate for V_{bi}.

We find for a series of cells with varying a-SiGe:H absorber layer thicknesses that V_{bi} = 1.17 V. This value is substantially larger than the typical open-circuit voltages (0.7 V) measured under solar illumination in these cells. It suggests that V_{bi} is not a substantial limitation to V_{oc} for cells with "narrow gap" absorbers.

UNI-SOLAR Code	*Thickness* (nm)	V_{oc} (V)	*FF*	*Optical Gap* (eV) (nominal)
LINE 10012 #22	220	0.955	0.705	1.7
LINE 10011 #32	150	0.794	0.63	1.55
LINE 10009 #33	150	0.699	0.558	1.50
LINE 10024 #22	140	0.65	0.549	1.45
LINE 10239	280	0.700	0.488	1.50
L 8692	1500	-	-	1.50
L 8693	1500	-	-	1.50
L 8702	1000	-	-	1.50

Table 1: Properties of eight Uni-Solar samples used in the present study. All of these cells have the structure ss/n^+/*i*/p^+/TCO (ss: stainless steel, TCO: transparent conductive oxide); n^+ layers are a-Si:H:P, p^+ layers are μc-Si:H:B.

Samples and Spectroscopic Details

The present work was done on two series of a-Si:H based *nip* solar cells prepared at United Solar Systems Corp.. Sample information is summarized in Table 1. The substrate material for these cells is stainless steel. All cells used comparable a-Si:H n^+ and μc-Si:H p^+ layers; samples varied in the thickness and bandgaps of the intrinsic absorber layers. For all but one of the samples, the absorber layer was based on a-SiGe:H alloys; one sample used unalloyed a-Si:H.

The actual measurement performed on these cells was electroreflectance. We used a beam from a monochromator to illuminate the specimen; the light reflected from top contact of the sample was detected using either a Si or an InGaAs diode detector. The reflectance was modulated by the reverse bias voltage across the cell. Since these cells have a top, anti-reflection coating, relatively little of the illumination is reflected from the first interfaces. For longer wavelengths, most of the illumination travels across the absorber layer. A substantial fraction (we estimate about 0.4) is reflected at the back stainless-steel contact. This back-surface reflected light travels back up through the absorber layer and exits the sample, following a path similar to that of directly reflected light. The Osaka University group, which did the pioneering work on V_{bi} estimation using electroabsorption,[3] dubbed this detection arrangement as "back surfaced reflected electroabsorption" (BASREA), since the intensity of the back-surface reflected beam is modulated by electric-fields through the electroabsorption effect. Of course the amplitude of the back-surface reflected beam interferes with the directly reflected beam, which may complicate optical analysis in some cases.

Electromodulated reflectance spectra $\delta R/(R\delta E)$ measured for the four thinnest cells are presented in Fig. 1. δE is the amplitude of the field modulation across the cell's absorber layer; all spectra were measured under 2 V reverse bias. One of the spectra is "unprocessed" and shows the extent of the interference

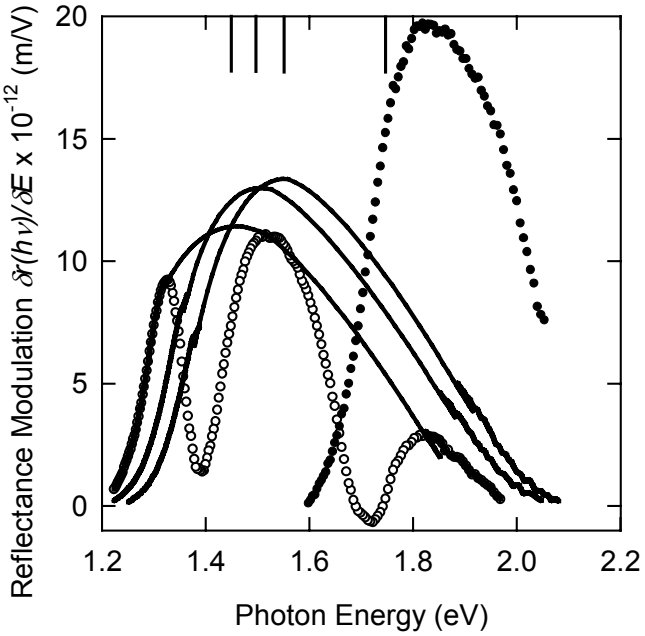

Fig. 1: Electromodulated reflectance spectra for four *nip* a-SiGe:H and a-Si based solar cells with varying absorber layer bandgaps. The "unprocessed" spectrum illustrates the large interference fringes resulting from superposition of back-surface reflected light with light directly reflected from the top layers of the cell. The remaining spectra are the upper envelopes of the unprocessed spectra.

fringes. The remaining spectra are the upper envelopes of the fringes, one of which corresponds to the unprocessed spectrum. Despite the ambiguities associated with the fringes, it is fairly evident that the peak of the spectra track the bandgaps of the absorber layers in the cells fairly well. The strengths of the electroabsorption spectra scale with the absorber layer thickness fairly well.

Built-in Potential Estimates

The essential measurement from which we estimate built-in potentials is the dependence of the electromodulation signal upon the DC potential drop V across the cell. Electroabsorption is quadratic with electric field in a-Si:H. Electromodulation essentially measures a derivative of the field-dependence, leading to the linear dependence upon V. We illustrate measurements for one sample in Fig. 2. The slope of the regression lines indicates the strength of the electroabsorption; the voltage-axis intercept V_0 is related to the built-in potential V_{bi} across the cell. The wavelengths selected for these measurements are those corresponding to maxima in the electromodulated reflection signal.

As is evident from Fig. 2, there is some dependence of V_0 upon photon energy. This dependence precludes an immediate identification of V_0 with V_{bi}. For the present measurements, it appears that a fairly simple effect is responsible. In Fig. 3 we illustrate the spectrum of V_0 for four samples with similar bandgaps and varying thicknesses. For the three thicker samples there is a common low energy limit of about 1.17 V. We believe that this value can be interpreted as V_{bi} for these cells. The thinnest sample, which also had a slightly lower bandgap, has a slightly smaller value in this limit.

For all four samples there is a transition to a substantially larger value for V_0 at shorter wavelengths. The thickness-dependence of the transition suggests that this effect is due to the change in the spatial origin of the electromodulation signal. For longer wavelengths the signal is sensitive to back-surface reflection of the incident light: interband optical absorption is fairly negligible. For shorter wavelengths interband absorption becomes much stronger, and the electromodulation signal is dominated by light reflected at the top of the cell. Indeed it is possible that the signal in this short-wavelength limit is dominated by the electroabsorption effect of the p^+ layer, since at the shorter wavelengths the electroabsorption strength is larger in the wider bandgap p^+ material than in the narrower bandgap intrinsic material. The most satisfactory view we have found is that this short-wavelength value for V_0 indicates the scaling of the field at the *p/i* interface. The numerical value for V_0 may be useful as a constraint on model calculations, but otherwise does not appear to be directly interpretable.

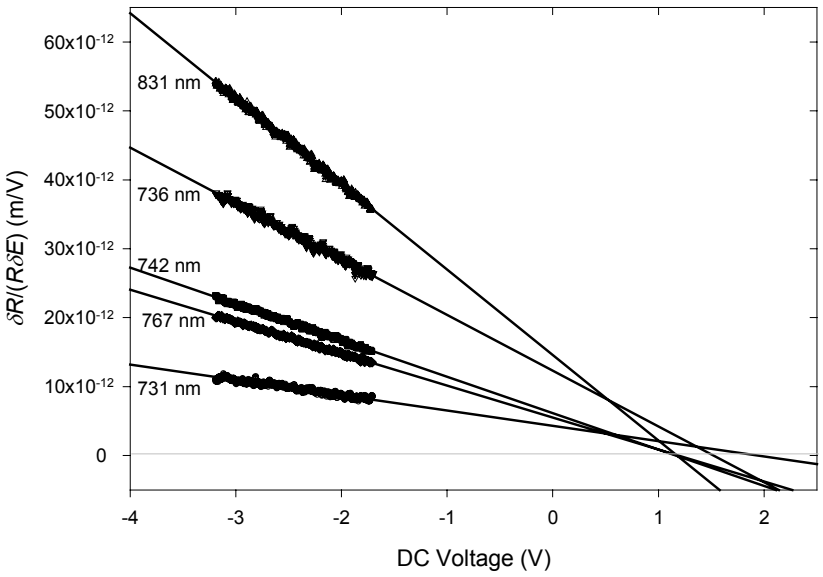

Fig. 2: Electromodulated reflectance signal $\delta R/(R\delta E)$ as a function of the external electrostatic potential across the cell for sample code L8702. Measurements are shown for several wavelengths along with linear regression lines.

Discussion

The value V_{bi} = 1.17 V we propose for cells with narrow bandgap (1.50 eV)

absorbers is larger than the value $V_{bi} \approx 1.05$ V which we have previously inferred for otherwise comparable cells with "ordinary" (1.75 eV) a-Si:H absorbers.1 It is somewhat smaller than our estimate $V_{bi} \approx 1.25$ V for cells with a-Si:H absorbers made with high hydrogen dilution.We have somewhat more confidence in the present measurements, for which we have not applied any corrections for the competition of the electroabsorption in the p^+ and intrinsic layers: there is relatively little overlap between electroabsorption bands for a narrow bandgap intrinsic layer and a microcrystalline *p*-layer.

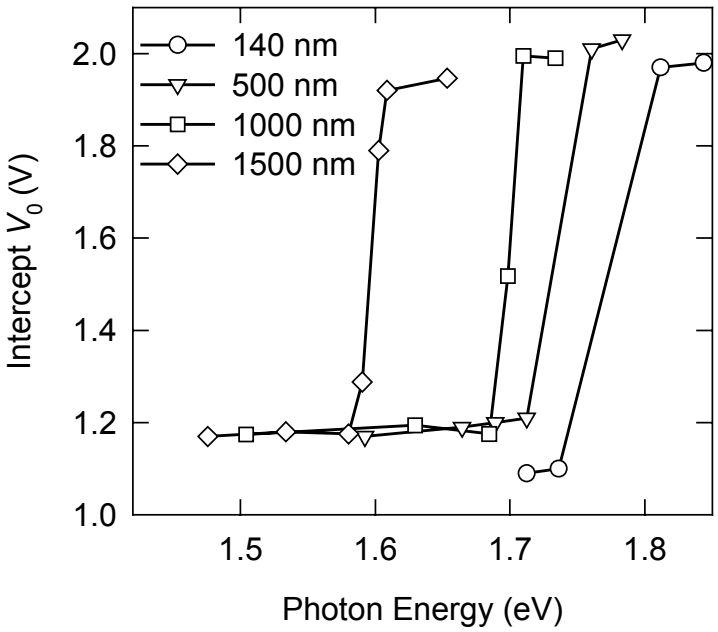

Fig. 3: Spectrum of the electroabsorption offset potential V_0 for four *nip* solar cells (prepared at USSC) with a-SiGe:H absorber layers of differing thicknesses; the typical optical gap was 1.5 eV. The low energy limit of about 1.17 V is an estimate of the built-in potential; open-circuit voltages ranged from 0.65 - 0.70 V under AM1 conditions. Sample codes (by thickness): (140 nm, L10024) (280 nm, L10239) (1000 nm, L8702) (1500 nm, L8692).

This variability is at least mildly surprising. Since the *n* and *p* layers of all of these cells are made with essentially the same recipes, and since one's first estimate for V_{bi} is simply the difference between the Fermi levels in these two doped layers, one might expect no variation due to changes in the the intrinsic layer separating the two doped layers. We have previously suggested that interface dipole effects reduce the built-in potential below the value which would be inferred from the properties of free-standing n^+ and p^+ layers. We still consider this entirely plausible; in addition to the electroabsorption measurements, there are several estimates of interfacial band offsets which, in our estimation, suggest interface dipole effects. Nonetheless it is only fair to note two difficulties. First, there is no obvious logic to the variability of V_{bi} for cells with varying absorbers. Second, the Urbana-Champaign group has failed to detect significant dipole formation in Kelvin probe studies of interfaces between doped and intrinsic layers formed using magnetron sputtering.[4]

Computer Modeling & Open-Circuit Voltages

Introduction

The open-circuit voltage V_{oc} of amorphous silicon (a-Si:H) based *pin* solar cells remains the most ill-understood of its device parameters. This lack of insight is remarkable, since the experimental behavior of V_{OC} is generally quite simple. V_{OC} depends little upon the defect density or thickness of the intrinsic layer, and eV_{OC} is roughly shifted down from the optical bandgap of this layer by about 0.8-0.9 eV. Furthermore, the value of V_{OC} is mostly controlled by the fairly simple physics of the splitting of quasi-Fermi-levels in the intrinsic layer. Nonetheless, even the simplest question about it, which is whether V_{oc} is reduced by non-ideal *p/i* or *n/i* interfaces, is not conclusively answered. Of course, this unsatisfactory state of affairs does leave open the tantalizing possibility of significant improvements in V_{OC} – if only device-makers could be pointed in a better direction.

In this section, we first review the interrelation of the open-circuit voltage and quasi-Fermi levels in the device physics of a-Si:H based *pin* solar cells. In cells with ideal *p* and *n* layers, V_{OC} reaches its "intrinsic limit," which may be equated to the splitting of the electron and hole quasi-Fermi levels in bulk intrinsic material. In principle V_{OC} measurements can become a very interesting alternative to photoconductivity measurements in intrinsic films. We next discuss the hypothesis that V_{OC} achieves this intrinsic limit for optimized a-Si:H cells, and we conclude that this hypothesis is most likely incorrect. First, open-circuit voltages do not exhibit the dependence upon defect density which is known to apply to quasi-Fermi levels for thin films of intrinsic a-Si:H. Second, we present electroabsorption measurements of the built-in potential in a-Si:H based solar cells which yield rather small values for V_{bi} (in the range 1.05 – 1.25 V). The built-in potential is generally recognized as the ultimate limit to V_{OC} in any solar cell. We present computer calculations which strongly suggest that the measured values are small enough to be reducing V_{OC} for the a-Si:H cells.

One unexpected result from the modeling work is that interface limitation can be significant even when V_{OC} is "significantly" (0.5 V) below the built-in potential. We present a computer simulation study of the mechanism by which non-ideal doped layers suppress V_{OC}, and we propose a "thermionic emission of minority carriers" model to explain the effect. The model shows that the conduction band offset between the *p* and *i* layers is as significant in determining V_{OC} and other cell properties as is the built-in potential V_{BI}.

V_{OC} and quasi-Fermi levels

In Fig. 4, we illustrate profiles for several important levels in an amorphous-silicon based *pin* solar cell under open-circuit conditions. The profiles are calculated using a computer program (AMPS PC-1D [5]) and parameters we describe in more detail subsequently. The upper panel is calculated under thermal equilibrium conditions (the dark), and shows the conduction and valence bandedges E_C and E_V, respectively, as well as the Fermi level E_F. The lower panel is calculated under illuminated conditions, and shows E_C, E_V, and the electron and hole quasi-Fermi levels E_{Fe} and E_{Fh}, respectively. By way of introduction, we now explain the equation between the measured open-circuit voltage under illumination and the separation of quasi-Fermi-levels. This well-known "theorem" proves to be a powerful tool in understanding open-circuit voltages in many solar cells which can be very well illustrated using computer calculations.

We briefly review the definitions of these levels. For an amorphous semiconductor, E_C is usually identified with a mobility-edge dividing extended electron states (at higher level energies) from localized *bandtail* states (at lower level energies). Electrons occupying extended states are assumed to be mobile, and are characterized by an electron "band mobility" μ_e. Electrons occupying the localized states are immobile (or *trapped*). This relatively simple model, in conjunction with the assumption that the bandtail states have an exponential distribution, accounts well for direct drift-mobility measurements for both electrons and holes. The electron quasi-Fermi level E_{Fe} is actually just a bookkeeping device for keeping track of the density of mobile electrons n under illumination [6,7]. Under thermal equilibrium (dark) conditions, we would calculate n from the expression $n = N_C \exp\left(-\left(E_C - E_F\right)/kT\right)$, where N_C is an "effective density-of-states" for the extended, conduction band states and E_F is the Fermi-energy. Under illumination, we define E_{Fe} implicitly from the definition: $n_{photo} = N_C \exp\left(-\left(E_C - E_{Fe}\right)/kT\right)$. Similar definitions apply to holes and the valence band.

Returning to Fig. 4, in the upper panel note the constancy of E_F (indicating that the different layers are in thermal equilibrium), and also note the decline in E_C across the cell. Spatial variation in E_C indicates that there is a "built-in" electric field driving electrons from left to right. The built-in field arises because electrons have been transferred from the *n* layer to the *p* layer in order to establish thermal equilibrium between the *n* and *p* layers, which have different Fermi energies relative to vacuum. The built-in potential V_{BI} is about 1.6 V for this calculation.

Under illumination, strongly non-equilibrium conditions are created. The middle portion of the cell becomes nearly free of electric field, and may be viewed as a slice of "bulk" intrinsic material. The zero of the vertical scale was set by the electron quasi-Fermi level E_F in the *n*-layer. E_{Fe} is essentially constant in the *n*-type and intrinsic layers. In the p-layer, there is a return to thermal-equilibrium conditions as indicated by the convergence of E_{Fe} and E_{Fh}. This effect arises from the much larger recombination rate of electrons in the *p*-layer *vis a vis* the intrinsic layer; there are far more holes trapped near E_{Fh} in the p-layer than in the intrinsic layer. A corresponding argument applies in the *n*-layer.

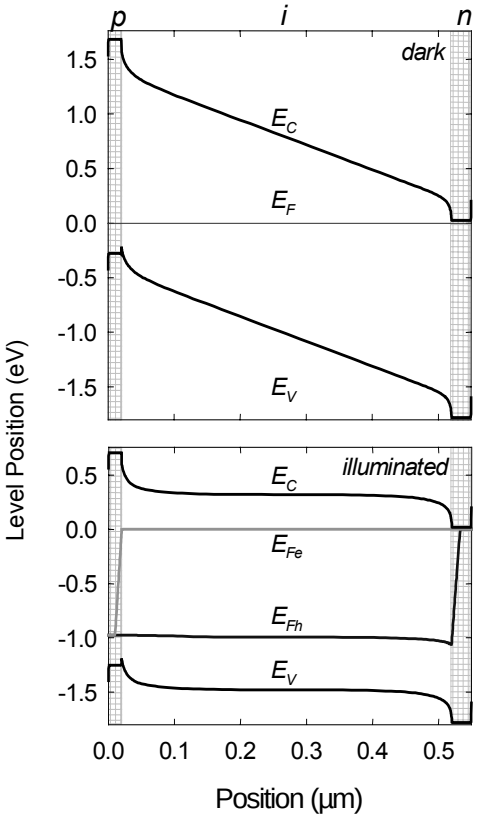

Fig. 4: Computer calculation of open-circuit profiles in an a-Si:H based *pin* solar cell for the conduction and valence bandedges (E_C and E_V) and of the Fermi level E_F (dark) or of the electron and hole quasi-Fermi levels (E_{Fe} and E_{Fh} - illuminated). The open-circuit voltage is precisely the value of E_{Fh} at the left interface ($x = 0$).

The *open-circuit voltage* V_{OC} is measured across the terminals of the cell; the computer calculation yields 0.99 V. V_{OC} may be equated to the difference in Fermi levels between the left and right termals of the cell:

$$eV_{OC} = \left(E_F(x_L) - E_F(x_R)\right) \ . \tag{1}$$

As can be seen from the figure, eV_{OC} is simply the difference between $E_{Fh}(0)$ and $E_{Fe}(0.55)$.

Is V_{OC} determined solely by intrinsic-layer properties?

For the parameter set used for Fig. 4: Computer calculation of open-circuit profiles in an a-Si:H based pin solar cell for the conduction and valence bandedges (EC and EV) and of the Fermi level EF (dark) or of the $_{electron}$ and hole quasi-Fermi levels (EFe and EFh - illuminated). The open-circuit voltage is precisely the value of *EFh* at the left interface (x = 0), interface effects are unimportant: quasi-Fermi levels are essentially constant throughout the cell, and there is a "field-free" zone in the middle of the cell. We conclude that, for these conditions, V_{OC} may be equated to the separation between the electron and hole quasi-Fermi levels E_{fe} and E_{Fh} for intrinsic films of a-Si:H:

$$eV_{OC} = \left(E_{Fe} - E_{Fh}\right) \ , \tag{2}$$

where *e* is the electronic charge [8]. We now attempt to establish whether this simplest case, that open-circuit voltages are determined simply by the photoconductivity of the intrinsic-layer material, applies in optimized a-Si:H solar cells.

V_{OC} depends weakly upon defect densities

It appears well accepted by device-makers that there is little correlation between V_{oc} and the density of deep levels N_D (usually presumed to be dangling bonds) in a-Si:H. One paper shows that the defect density in intrinsic films could be increased nearly thirtyfold by light-soaking, while V_{OC} diminished by about 0.03 V [9].

The expected decrease in V_{OC} as the defect density changes may be calculated from the changes in the quasi-Fermi-levels for electrons and holes. The corresponding decline in the photoconductivity of a-Si:H films is roughly proportional to the reciprocal density [10]. Since the photoconductivity is electron-dominated, one may estimate the decline in the electron quasi-Fermi level ΔE_{Fe} simply:

$$\Delta E_{Fe} \Big/ kT = \ln\left(N_D^f \Big/ N_D^i \right) \ . \tag{3}$$

One obtains an expected decline of V_{OC} of about 0.09 eV due to this effect, which is substantially larger than the observed decline. A smaller effect which further reduces V_{OC} is due to changes in the hole quasi-Fermi-level E_{Fh} as the defect density rises.

It is clear that the myriad of photoconductivity measurements on a-Si:H have at best an uncertain relationship to V_{OC}. The alternative is that V_{OC} is determined by photoconductivity effects in the interface regions. Indeed the present argument favoring interface effects would be conclusive if defect density changes as large as those in films were observed in *pin* cells, but effects this large have not (to our knowledge) been reported.

Crossover from intrinsic to interface limitation of V_{OC} is not abrupt

The simplest perspective on interface limitation of V_{OC} is the following. It is reasonable that V_{OC} cannot exceed V_{BI}; inspection of Figure 1 shows that V_{OC} is reduced from V_{BI} by electrostatic barriers at each interface. One might therefore guess that, for low photogeneration rates G, V_{OC} should be dominated by intrinsic-layer quasi-Fermi-levels; for higher photogeneration rates there will be a crossover to the value $V_{OC} \approx V_{BI}$.

This perspective is profoundly misleading, as we now illustrate. Crossover from intrinsic-layer to interface limitation of V_{OC} occurs over many orders of magnitude of G, and can set in when V_{OC} is much below V_{BI}.

In Fig. 5 we present calculations of V_{oc} for varying (uniform) photogeneration rates. We chose band and bandtail parameters based on a variety of fundamental measurements; the details are presented in the Appendix. For these calculations, intrinsic layer defects were not incorporated, since V_{OC} is not much affected by them. The uppermost, solid bold line is the result of an analytical calculation developed by Tiedje some years ago [11] which exploits the equation of V_{OC} with quasi-Fermi level splitting in the intrinsic layer. This calculation establishes what may be termed the *intrinsic limit* $V_{OC}^{intrinsic}$, by which we mean the upper limit determined only by the photoconductivity of the intrinsic layer itself.

For the AMPS calculations, the *n*-layer Fermi energy was set 0.1 eV below the conduction band, and had the same bandedges as the intrinsic-layer. We expect these parameters to adequately model a-Si:H:P *n*-layers. The *p*-layer bandgap was set to 1.96 eV, with symmetrical 0.08 eV offsets between the p-layer and intrinsic-layer bandedges. These parameters nominally describe a-SiC *p*-layers. The *p*-layer Fermi energy was adjusted to yield the several values of the built-in potential shown in the figure. The points calculated for V_{bi} =1.52 V approach the results of the analytical calculation for V_{OC} based on intrinsic layer properties alone. The consistency between the analytical and computer calculation is noteworthy.

Built-in potentials are small enough to affect V_{OC}

The points for V_{bi} = 1.32 V fall away significantly from the intrinsic-layer limit due to interface limitation by the *p/i* interface. We note two aspects of this behavior. First, interface limitation is important even when V_{OC} is substantially (0.4 V) less than V_{bi}. Second, the power-law, functional form of the dependence of V_{oc} upon G gives little indication that V_{OC} has been reduced by the interface. The crossover from intrinsic limitation (at

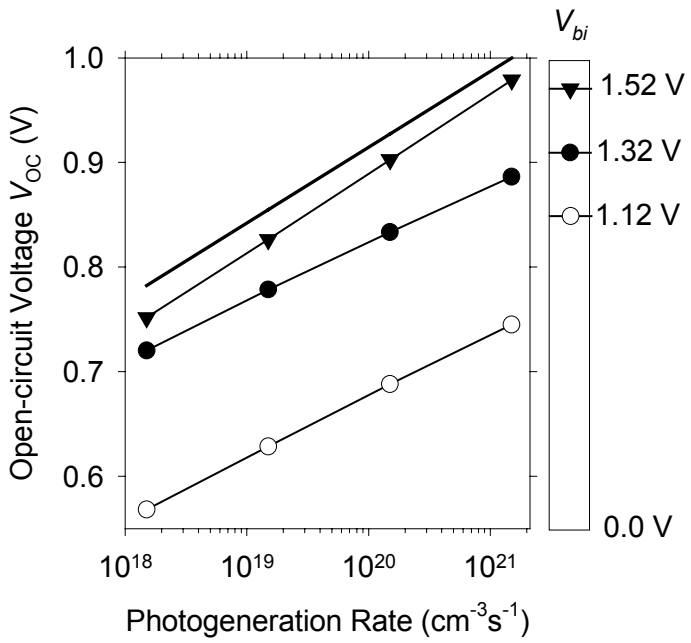

Fig. 5: Calculations of the dependence of the open-circuit voltage upon photogeneration rate for *pin* solar cells. The bold solid line is an analytical calculation based on intrinsic layer properties alone. The symbols plotted for different V_{bi} are based on computer calculations for varying Fermi-energies in the *p*-layer.

low G) to interface limitation (at high G, as V_{OC} begins to approach V_{BI}): the interface causes an extremely soft effect on V_{OC} which is stretched over many decades of generation rate.

Does the p-layer reduce V_{OC} in optimized a-Si:H devices? To our knowledge, the best elaborated experimental estimates of V_{bi} in a-Si:H based *pin* solar cells are based on the small, electroabsorption effect [12]. In practice, one measures the modulated transmittance S due to sinusoidal modulation δE of the electric field across the cell. This signal depends linearly upon the constant, DC voltage V across the cell:

$$S \propto \delta E\left(V - V_0\right) .$$

Note that there is an offset voltage V_0. Under ideal conditions, V_0 determines the "built-in" potential.

In Fig. 3 we presented a summary of the results for V_0 as a function of the wavelength for a series of *pin* cells incorporating a-SiGe intrinsic layers with varying intrinsic-layer thicknesses and bandgaps; the cells were prepared at United Solar Systems Corp.. The doped layers were deposited under the same conditions for all of these cells. The *n*-layer was a-Si:H:P; the *p*-layer was microcrystalline Si:B [13].

A full interpretation of these measurements is more complicated than the simplified description above implies, and will not be given here. For these cells the optical measurements were actually reflectance, not transmittance. For smaller optical energies incident illumination travels through the cell and is reflected at the back surface; the measured reflection modulation is dominated by the back-surface reflected beam. As can be seen in the figure, several cells yield $V_0 \approx 1.15$ V in this regime. For shorter wavelengths the incident beam is too strongly absorbed to reach the back surface, and the measured signal is essentially true electroreflectance. We have not yet found a convincing explanation for the value $V_0 \approx 2.0$. From these data and our prior work, we conclude that $1.05 < V_{BI} < 1.25$ for the range of cells we have studied, including our work with both microcrystalline Si and amorphous SiC p-layers.

In conjunction with the simulation results in Fig. 5, this range of values for V_{BI} is plainly small enough to suggest that V_{OC} is probably reduced by the *p/i* interface in working cells. In the next section we present a discussion of the device physics which underlies this effect.

Device Physics of the *p/i* Interface

In Fig. 6 we present open-circuit profiles for an AMPS calculation with the parameters of Fig. 5 ($V_{bi} = 1.32$ V, $G = 1.5\times10^{21}$ cm^{-3}). As can be inferred from the bottom right panel of the figure, the diminishment is associated entirely with the gradient $e\Delta V^{p/i}$ in E_{Fh} as it crosses through the *p/i* interface: the separation between E_{Fe} and E_{Fh} in the central, field-free zone remains at its intrinsic limit of about 1.0 V.

Non-constant profiles for E_{Fh} imply the existence of a corresponding hole current, in this case flowing from the intrinsic layer into the *p*-layer. We show the corresponding electron and hole current profiles in the figure also; since there is no net electrical current flowing under open-circuit conditions, the electron and hole currents cancel exactly. The fact that the electron current flows without an appreciable gradient in E_{Fe} reflects the facts that E_{Fe} is closer to its band than E_{Fh}, as well as the larger band mobility chosen for electrons.

These currents reflect the transport of electrons and holes which are photogenerated in the intrinsic layer into the *p*-layer, where they recombine quite close to the interface. Indeed the recombination current at the interface is readily computed from the sharp drop in J_e and J_h.at the interface. We were initially surprised by the existence of the electron current. As illustrated in the figure, there is a sizable electrostatic barrier W which impedes electron current into the *p*-layer.

These currents may be understood in terms of thermionic emission of electrons over the barrier W. In Fig. 7 we show the logarithm of the recombination current as a function of the barrier height W. Currents associated with a given symbol were calculated by varying W using only the conduction band offset at the *p/i* interface $\Delta E_C^{p/i}$; all other parameters were unchanged. Different symbols correspond to different photogeneration rates; these change W by changing the electron quasi-Fermi level E_{Fe} in the intrinsic layer.

For a specific illumination, J_R is activated for larger barrier heights; the decline illustrated in the figure is consistent with $J_R \propto \exp(-W/kT)$. For smaller barrier heights, J_R is limited by the total photogeneration within a certain range from the *p/i* interface; we speculate that this range is the ambipolar diffusion length.

In Fig. 8 we present the dependence of V_{OC} upon photogeneration rate G for the same calculations used for Fig. 7. We varied the band offsets $\Delta E_C^{p/i}$, and left the built-in potential constant at 1.2 V. Note the very large range of generation rates involved. For the larger values of $\Delta E_C^{p/i}$, V_{OC} lies on the *intrinsic limit* line throughout the range of G. However, as $\Delta E_C^{p/i}$ declines, V_{OC} breaks away progressively; V_{OC} is significantly diminished from the intrinsic limit $V_{OC}^{intrinsic}$ throughout the normal range of photogeneration rates, and adopts essentially the same power-law form as for the intrinsic limit.

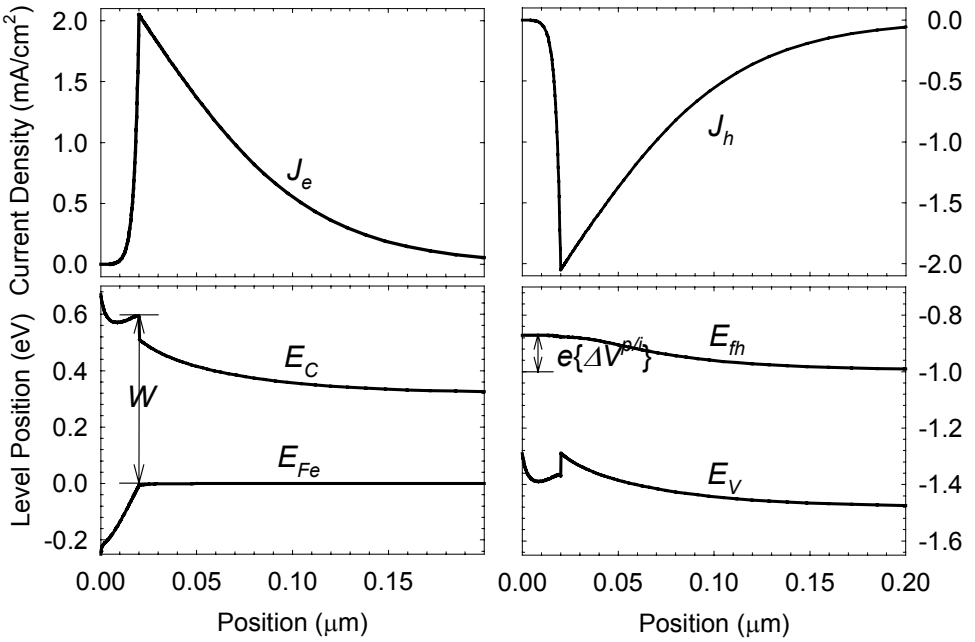

Fig. 6: Profiles calculated using AMPS and the common parameters described in the text. The built-in potential was set to 1.3 V by adjusting the doping level of the *p*-layer. Note the electron current J_e, which is a consequence of thermionic emission over the barrier W. While J_e flows without an appreciable gradient in E_{Fe}, the hole countercurrent J_h does require a noticeable gradient $e\Delta V^{p/i}$.

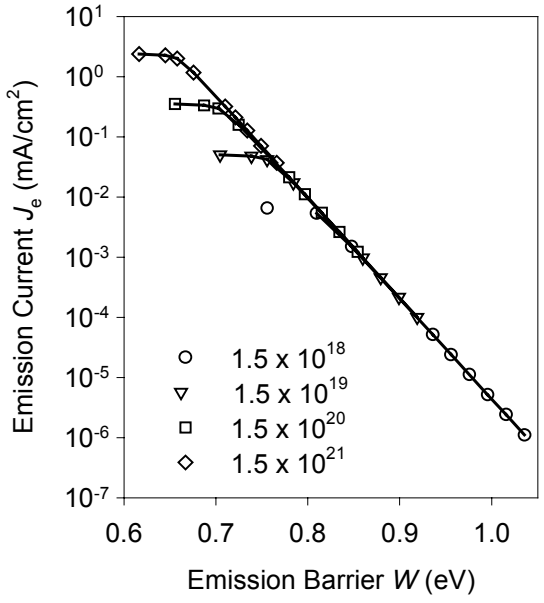

Fig. 7 Dependence of the electron current J_e at the *p/i* interface upon the barrier height W (see figure 4) for several different uniform generation rates. For each intensity, W was varied by changing only the conduction band offset at the *p/i* interface; V_{BI} = 1.2 V.

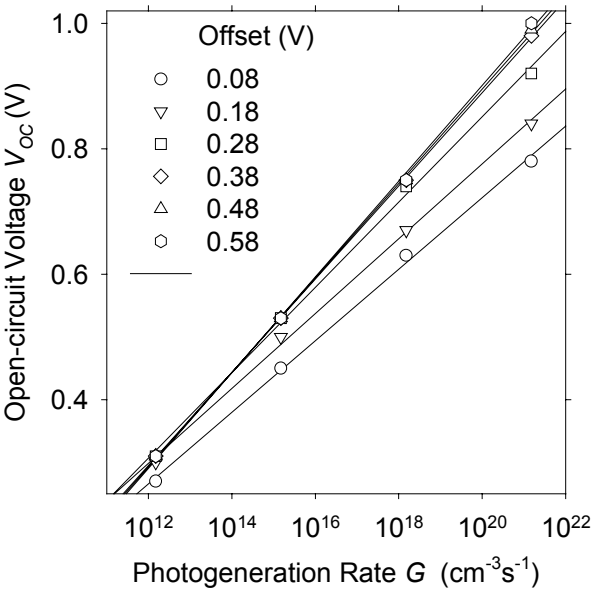

Fig. 8: Open-circuit voltage V_{OC} as a function of (uniform) photogeneration rate G; results for varying conduction band offset $\Delta E_C^{p/i}$ are given. Note that the built-in potential V_{BI} = 1.2 V does *not* change for these calculations.

Discussion

We have presented two results which militate against the simple model that open-circuit voltages achieve their intrinsic limit $V_{OC}^{\text{int}rinsic}$ in a-Si:H based *pin* solar cells. First, the unexpected robustness of V_{OC} as defect densities in the intrinsic layer are increased seems inexplicable in this model. Second, experimental estimates for V_{bi} are sufficiently small that, in conjunction with computer modeling of a-Si:H based cells, they argue for interface limitation of V_{OC}. To these results may be added other experiments which show that modification of the p/i interface region by inclusion of "buffer layers" of various types increases V_{OC} [14].

What is plainly required to advance open-circuit voltage physics is a satisfactory model for V_{OC} based on interface physics. We have developed a fairly satisfactory account for the computer calculations of *p/i* interface effects in terms of electron thermionic emission from the intrinsic layer into the *p*-layer which we believe can form the basis of an improved model. Nonetheless, we cannot claim at present to have a satisfactory understanding of V_{OC}. For example, the measured slopes of the logarithmic, V_{OC} vs. photogeneration rate in cells are steeper than the results of the computer calculation. We are, reluctantly, considering the possibility of more complex models for the *p/i* interface than the simple "heterostructure" model treated here. As one example, Branz and Crandall [15] have discussed thermodynamic defect generation at the *n/i* and *p/i* interfaces.

Appendix: bandtail parameters for solar cell modeling

This page contains a set of parameters based on the literature of direct experiments on photocarrier and optical processes in intrinsic amorphous silicon.

Parameter	*AMPS Symbol*	*Value*	*Notes and References*
Overall Electronic Properties			
Electrical Bandgap E_G	EG	1.80 eV	This parameter is surprisingly difficult to establish accurately; the best estimates appear to be those based on internal photoemission: Chen and Wronski [16].
Conduction Band Parameters			
Effective density of states N_C	NC	2.5×10^{20} cm^{-3}	Jackson, *et al.*[17] did a careful study of photoemission and related measurements, and suggested that *g(E)* near E_C (the conduction band mobility edge) is about 10^{22} cm^{-3}. N_C is roughly the product of *kT* and this value for *g(E)* near room-temperature.
Electron band mobility μ_e	MUN	2 cm^2/Vs	Schiff, *et al.*[18] found that this value applies from essentially the moment of photogeneration throughout the picosecond domain. Larger values can be excluded both from this work and work by Juska, *et al.* [19].
Bandtail width	EA0	0.022	Wang, *et al*.[20].
Bandtail prefactor	GA0	10^{22} $cm^{-3}eV^{-1}$	See notes on NC. Note that NC = (kT)*GA0.
Bandtail cross-section ($B^0 + e^-$ -- B^-)	TSIG/NA	2×10^{-16} cm^2	Wang, *et al.*[20] estimated $\nu = 5x10^{11}$ s^{-1} for the "attempt-to-escape" frequency governing electron emission from the bandtail. "Detailed balance" $\nu = N_C b_T$ then constrains TSIG/NA, since b_T = (TSIG/NA)v_{thermal}.
Bandtail cross-section ($B^- + h^+$ - B^0)	TSIG/PA	10^{-16} cm^2	It is possible that this parameter has little effect on solar cell models. Nonetheless, we are not aware of any satisfactory experimental estimate of it. One might apply the "Langevin" expression for diffusion-limited capture of a free hole by a negatively-charged center, yielding perhaps $2x10^{-14}$ cm^2 [21]. This procedure doesn't work for electron capture by trapped holes, however.
Valence Band Parameters			
Effective density of states	NV	2.5×10^{20} cm^{-3}	cf. Jackson, *et al.*[17]; see note for NC.
Hole band mobility	MUP	0.27 cm^2/Vs	Gu, *et al.* [22] have collected hole drift-mobility measurements and suggested this fitting for "standard" a-Si:H.

Parameter	*AMPS Symbol*	*Value*	*Notes and References*
Bandtail width	ED0	0.048 eV	Basically set using Urbach tail. This value is conventional; see Gu, *et al.* [22] for estimates based on hole drift mobilities.
Bandtail prefactor	GD0	10^{22} $cm^{-3}eV^{-1}$	Jackson, *et al.* [17]. See note for NV.
Bandtail cross-section ($B^0 + h^+$ -- B^+)	TSIG/PD	3×10^{-17} cm^2	Based on NU = $7.7x10^{10}$ s^{-1} from Gu, *et al.* [22]. See note for TSIG/NA
Bandtail cross-section ($B^+ + e^-$ -- B^0)	TSIG/ND	10^{-16} cm^2	Juska, *et al.* [23] have inferred this parameter from subnanosecond recombination experiments. A slightly larger value was reported by Stradins, *et al.* [24]. These values are much smaller than expected from a fundamental argument due to Langevin; no one seems to understand the reason for such small values (see Schiff [21]).

A note about capture cross-sections

It is conventional, and regrettable, that capture rates of photocarriers into localized states are described using cross sections. Rates for capture of a photocarrier are usually written in the form $R = bN$, where N is the density of some type of level which captures photocarriers, R is the capture rate (in s^{-1}), and b is the "capture coefficient" (in cm^3s^{-1}). It is conventional to express b in terms of a cross section $b = \sigma^* v_{th}$, where σ is the capture cross-section (in cm^2) and v_{th} is a "thermal velocity." This last expression is a legacy from atomic scattering, and is probably meaningless in amorphous silicon. By convention we simply take $v_{th} = 10^7$ cm/s and don't think about this further.

Hole Drift Mobilities in a-Si:H: Maximal Hydrogen Dilution and Related Samples

Introduction

Thin-film silicons made using silane gas diluted with hydrogen have structures ranging from amorphous to microcrystalline; a transition occurs as the hydrogen dilution is increased [25]. Amorphous silicon layers made at the maximal dilution for which an amorphous structure is retained have several interesting properties. First, they tend to have slightly larger optical bandgaps than lower-dilution amorphous materials, which makes them potentially useful for preparing high V_{OC} cells. Second, there is some evidence that maximal-dilution materials have better stabilized electronic properties than low-dilution materials. These properties must of course be considered in the context of the lower deposition rates for layers as hydrogen dilution increases.

Hole Drift Measurements

In Fig. 9 we show the temperature-dependence measured of the hole drift-mobilities for two samples of H-diluted a-Si:H along with previous measurements on triode-deposited a-Si:H, hot-wire a-Si:H [26], and a regression fit from hole measurements in conventional a-Si:H [27]. These drift-mobilities apply for a specific ratio $L/E = 2 \times 10^{-9}$ cm^2/V of hole displacement L and field E.

We have measured hole mobilities in three a-Si:H samples made at high dilution by Prof. Christopher Wronski's research group at Pennsylvania State University. The a-Si:H layers are deposited on SnO_2-coated glass (Corning 7059). The structure of the samples is glass/SnO_2/a-Si:H:P (n+)/a-Si:H (i)/Ni. The

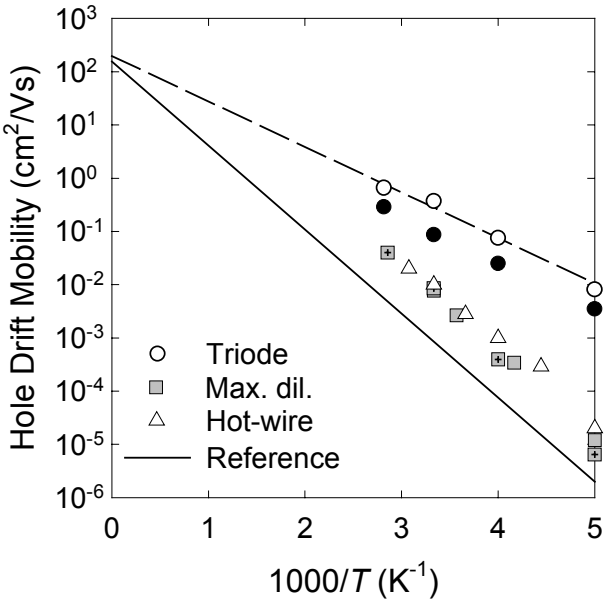

Fig. 9: Temperature-dependent hole drift mobilities for several a-Si:H samples ("triode" – deposited at Electrotechnical Laboratory, "max. dil."-maximal hydrogen dilution deposited at Penn State University, "hot-wire" deposited at National Renewable Energy Laboratory; reference deposited at United Solar Systems Corp.. Values are given for a displacement/field ratio $L/E = 2\text{x}10^{-9}$ cm^2/V;

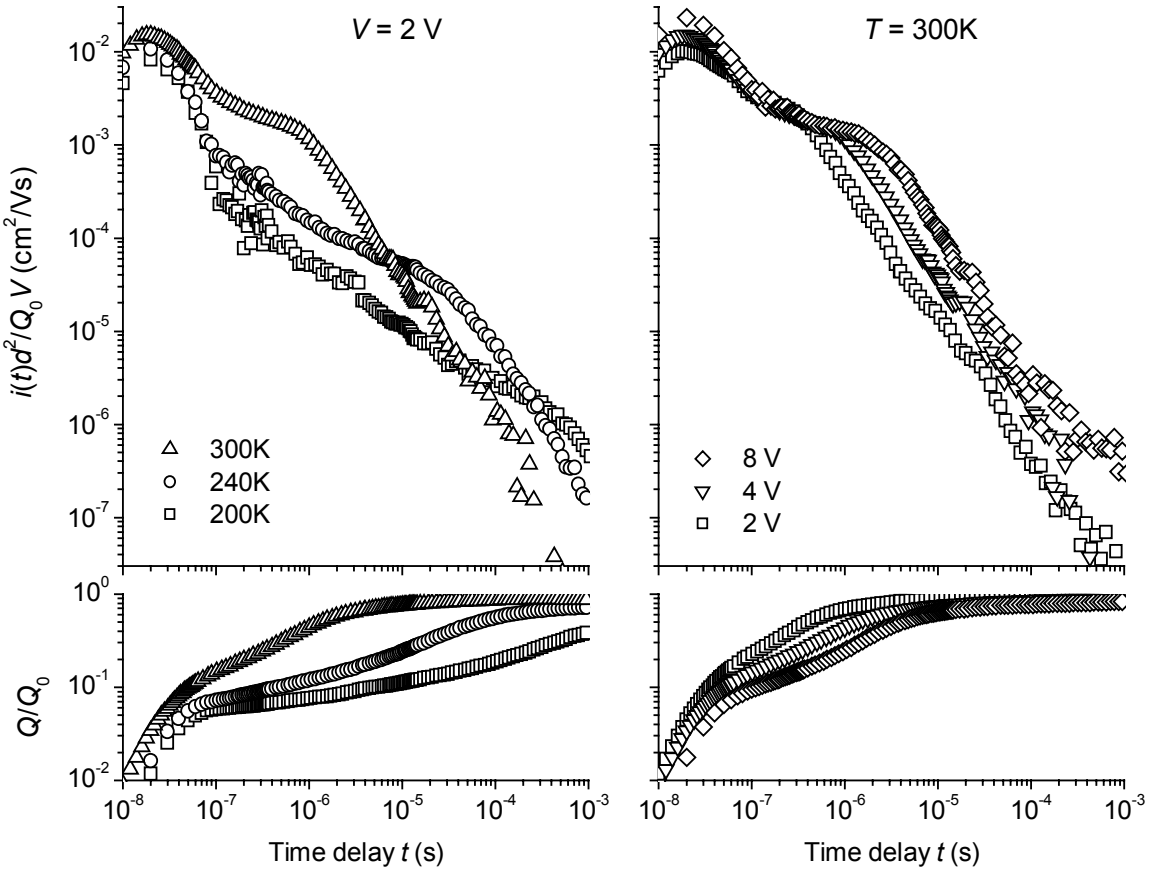

Fig. 10: Transient photocurrent $i(t)d^2/Q_0V$ and photocharge $Q(t)/Q_0$ due to holes for an a-Si:H sample made at high hydrogen dilution at Pennsylvania State University. Q_0 is the total photocharge measured at 10^{-3} s with 8V at 300 K. Note that the photocharge for longer times is unchanged by voltage at 300 K, but that full collection of photocharge does not obtain at 200 K. Note also that the normalized photocurrent is voltage independent at shorter times at 300 K; the transient for longer times exhibits sweepout of the photocharge to the electrodes. Drift mobility estimates are obtained from these curves.

a-Si:H layers were deposited using a Tek-Vak MPS 4000-LS multi-chamber PECVD system. The intrinsic-layer deposition was done using a substrate temperature of 200 C and a hydrogen/silane ratio of 10:1. (200 C, R=H_2/SiH_4=10:1). The n+ layer was 35 nm thick and has an activation energy for electrical conduction of 0.25 eV. A top semi-transparent Schottky barrier was formed by thermal evaporation of Ni onto the intrinsic layer immediately following a short etching with buffered hydrofluoric acid; small, circular Ni electrodes of area 0.02 cm^2 were formed; the thickness of the Ni films was 15 nm.

Three different samples were prepared over several months; the sample codes and their thicknesses are (CW81 - 1.1 microns, PSU 020299R – 1.5 microns, PSU 031599R - 1.47 microns). We illustrate the hole photocurrent transients measured on the third and last of these samples in Fig. 10. The transients are not remarkable, and are typical of "time-of-flight" measurements in amorphous-silicon based materials.

Fitting to the Exponential Valence Bandtail Trap Model

We have made a careful fitting study of these data using the well-known exponential bandtail trapping model [22]. As may be recalled, the three parameters of this model are the width parameter E_0 describing the exponential valence bandtail, the "attempt-to-escape" frequency ν describing hole emission from a bandtail trap, and the "microscopic mobility" μ_0 describing free drift of an untrapped hole. We

summarize our fittings in the table below for the three hydrogen-diluted samples studied. We also report values from our earlier work on holes [22]. The parameters ν and μ_0 are unremarkable; they are rather difficult to establish accurately from the drift-mobility measurements, and are typically much less reproducible than the drift-mobility measurements themselves. In this context it is quite possible that the variations in the table are not significant. On the other hand, the valence bandtail width E_0 is relatively easy to establish, and indicates that the width is narrower for the hydrogen-diluted materials than for conventional amorphous silicon materials.

In previous work we found little variation of the hole drift-mobility with alloying of the amorphous silicon with germanium or with carbon, although electron drift-mobilities do vary significantly with alloying. It appears that increase in the "order" or "protocrystallinity" of amorphous silicon when it is deposited under conditions of high-hydrogen dilution have essentially the reverse effect: there is a noticeable narrowing of the valence bandtail width.

We have not determined whether the Urbach energy determined from optical absorption measurements corresponds to the bandtail width determined by hole time-of-flight in hydrogen-diluted materials. In conventional a-Si:H samples, the correspondence is rather good: the Urbach edge is about 48 meV, as is the bandtail width. However, for a-SiC materials there was essentially no correlation between the Urbach energy and the bandtail width [22]; the lack of correlation has never been explained.

Sample	E_0 (meV)	ν (s^{-1})	μ_0 (cm^2/Vs)
Hydrogen-diluted (PSU-CW81)	40	6.3×10^{11}	0.2
Hydrogen-diluted (PSU-2)	39	1.0×10^{12}	0.3
Hydrogen-diluted (PSU 031599R)	42	2.0×10^{12}	0.6
Conventional (ECD 1689)	48	7.7×10^{10}	0.27

Table I: Exponential bandtail multiple-trapping fitting parameters.

Interface Absorption Spectroscopy

Introduction

For the last few years we have been developing an infrared modulation spectroscopy technique that probes the optical spectra of dopants and defects at the critical interfaces between the layers of amorphous silicon *pin* solar cells [28,29,30]. We are, of course, interested in adding to the information available from better-known methods, including *in situ* optical and photoemission studies of films as they are grown [31,32], and *ex situ* measurements on working cells such as *internal photoemission* studies (which establish band offsets) [33] and *capacitance spectroscopy* (which probes the density of interface states) [34].

In the present paper we describe our work with an modulation spectroscopy technique which probes the optical spectra of dopants and defects at the interfaces to the intrinsic layer in working cells. The technique itself has been described previously [35,36]. In brief, the reverse bias voltage across a cell is sinusoidally modulated, and the corresponding modulation of an optical measurement (transmission or reflection) is detected. We illustrate such spectra as Fig. 11 and Fig. 12, where the modulation spectrum $\Delta T/T$ of the optical transmission through a *pin* solar cell is shown. The principal feature in these spectra is the large peak near 1.85 eV; this feature, which depends upon the magnitude of the DC potential V_{DC} across the cell, is due to the well-known *electroabsorption* effect in the intrinsic, a-Si:H layer of the cell [37]. The much weaker infrared signal is nearly independent of V_{DC}, and is attributed to the change in optical transmission as the *charge state* of dopants and defects near the interfaces is modified by the sinusoidal modulation of the electric potential across the cell. The electroabsorption effect is quadratic in electric field, which leads to a signal quadratic in the modulated field and V_{DC}. The interface effect varies with the charge modulation at the interfaces, and is independent of V_{DC} when the capacitance is also

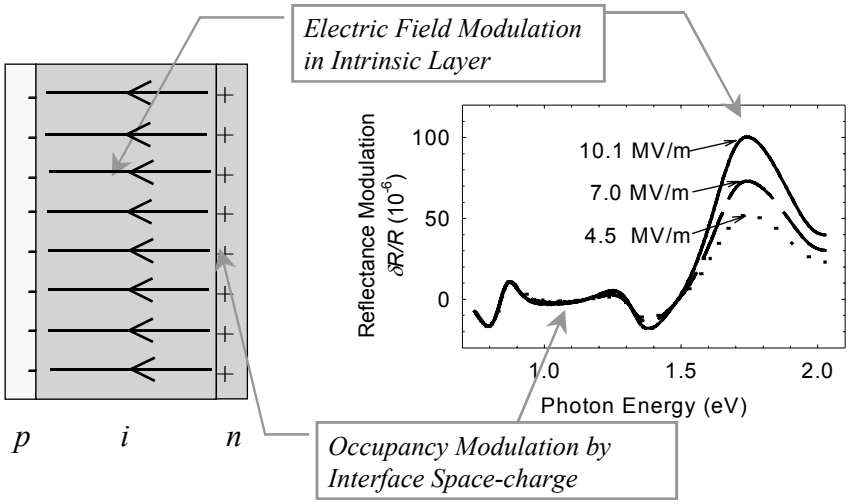

Fig. 11: The figure illustrates the interpretation of the electromodulation spectrum's two regions based on their very different scaling with reverse bias. For constant modulation amplitude, the interband electromodulation spectrum near 1.8 eV scales linearly with applied bias voltage, corresponding to true, quadratic electroabsorption in the intrinsic layer. The infrared spectrum is nearly independent of the bias, as expected from effects originating from occupancy changes near the interfaces. The sample was a pin diode for which electromodulated reflectance was measured. These spectra are affected by interference between back and front-surface reflection; ref. [40] shows spectra on additional samples without interference.

independent of V_{DC}. For later reference, note that a positive signal in the spectra indicates that increasing depletion of the *n* and *p* layers decreases the transmission through the sample.

In the remainder of this section we report measurements of the infrared, interfacial effect for six specimens, and we discuss the origins of these spectra in terms of the optical properties of dopant and defect levels near the interfaces. In the following two sections we discuss the defect complexing model, and then we describe an experiment in which we used optical bias in an effort to distinguish the *p/i* and the *n/i* interface spectra.

Transmittance Measurements

In Fig. 13 we present transmittance modulation spectra for six different samples. We describe the samples in more detail subsequently. The modulated transmittances $\Delta T/T$ has been normalized by the areal density ΔN of charges induced by the potential modulation; the spectra have the dimensions of an optical cross-section.

The samples prepared at the National Renewable Energy Laboratory (NREL) were designed to find out whether the interface spectra depended upon the density of dopants in the *n*-layer of a *pin* cell. All layers were prepared by plasma deposition; the substrates were glass which was coated with transparent, smooth conducting oxide (TCO). The *p*-type and intrinsic layers were a-Si:H; the intrinsic layer was about 1000 nm thick. One sample had a heavily doped *n*-type layer (1% PH_3 in SiH_4). The second sample (denoted *pi vn*) had a rather thick (300 nm), lightly-doped layer (0.005% PH_3 in SiH_4) interposed between the intrinsic layer and heavily doped layers. The charge induced by voltage modulation is primarily in the lightly doped layer. The modulation spectra exhibit strong interference fringes. While we have not done a complete optical analysis, it appears that the modulation spectrum is dominated by the effects of the slight change in optical phase of light reflected or transmitted near the charged interfaces; this phase effect is evidently strongest near 0.8 eV and decays slowly up to at least 1.5 eV. There must also be a corresponding absorption effect, but we aren't able at present to clearly distinguish absorption in these spectra. The sample with the lightly-doped n-type layer has a weaker spectrum; we return to the differences between these two samples in the next section describing reflectance experiments.

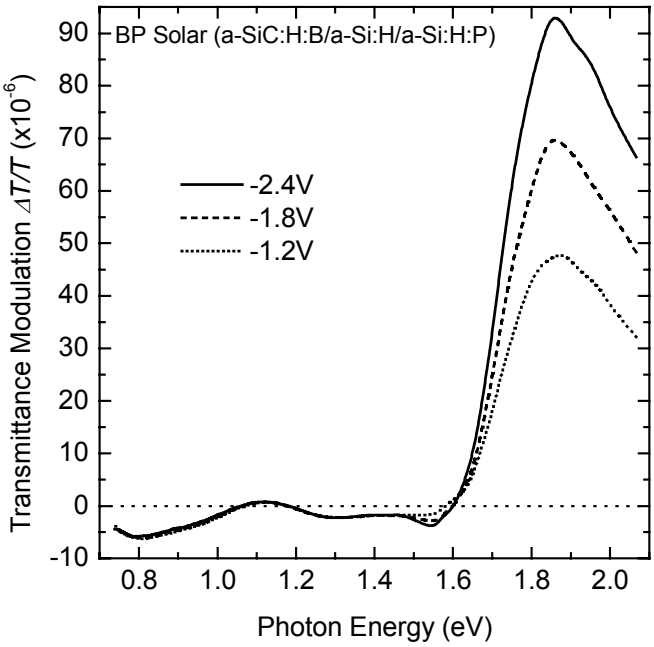

Fig. 12: Transmittance modulation spectrum $\Delta T/T$ for an amorphous silicon-based *pin* solar cell prepared at BP Solarex. The larger, voltage-dependent peak near 1.8 eV corresponds to *interband electroabsorption*. The weak, *negative* infrared response is due to charging and discharging of dopant and defect levels near the *n/i* and *p/i* interfaces. Measured with 20 kHz, 1.6 V_{pp} modulation.

The two samples from the Institute for Energy Conversion (IEC) were prepared on TCO coated substrates using amorphous (a-Si:H:P) and microcrystalline (μc-Si:H:P) *n*-type layers. The intrinsic layers were 500 nm thick. The devices had no *p*-type a-Si:H layers; top TCO layers were the electrodes. The broad spectral feature for the amorphous *n*-layer appears consistent with the measurements on NREL diodes.

The samples prepared at BP Solarex were deposited onto glass coated with textured SnO_2. The *p*-type layer deposited onto the SnO_2 was a-SiC:H:B, followed by a-Si:H. Two types of *n*-type layer were used (amorphous (a-Si:H:P) or microcrystalline (μc-Si:H:P)). As is evident, these spectra are very different from those of the other diodes. Because of the textured substrate, we do not expect strong interference fringes. We speculate that the "microcrystalline" material at the *n/i* interface was more completely microcrystalline for the BP Solarex sample than for the IEC sample, thus explaining its very different spectrum (including a change in sign of the modulation signal). The spectra for the IEC structures suggest that a substantial volume fraction of the microcrystalline material right at the *n/i*-inteface remained amorphous; the statement is based on the similarity in the signals from the cells with purely amorphous and with microcrystalline *n-layers*. The spectrum for the BP Solar sample with an amorphous *n*-type layer surprises us, and we do not currently have a satisfactory explanation for it.

Reflectance measurements

We also performed modulated reflection measurements on the two NREL samples; these are presented in Fig. 14. The three different reflection spectra correspond to reflection measured with light incident on the *n/i* and *p/i* interfaces of the device with a heavily doped *n*-layer, as well as for light incident on the *v/i* interface of the device with the lightly doped *n*-layer.

The most interesting feature of these spectra is the rather strong, sharp feature near 0.8 eV for reflection of light incident on the *n/i* interface. We believe that this feature is due to the change in the *absorption* of doping and defect levels as their charge state changes. It surprises us somewhat that this feature is much less obvious for reflection studied with illumination incident through the *p*-layer; since the intrinsic-layer is quite transparent at these photon energies, one expects to see the effects of changes in either interface in reflectance from either side of the structure. We have not done the more detailed optical analysis required to discuss these issues further.

It is noteworthy that this sharp feature is missing from the modulated reflection for the *v/i* interface; although the interface charges are spread out through a greater depth in lightly-doped *n*-type material, it is surprising that the optical effect per charge changes. We discuss possible origins for this effect in the next section.

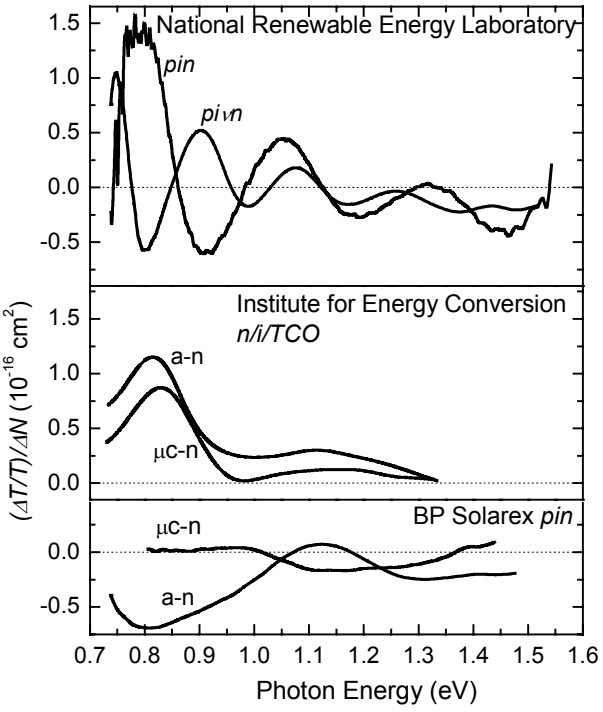

Fig. 13: Spectra of the transmittance modulation $\Delta T/T$ due to a sinusoidal voltage across several a-Si:H based solar cells and diodes; the modulation has been normalized by the areal density ΔN of charges deduced from simultaneous capacitance measurements.

Discussion

There are two insights which may be gained from the present measurements. First, it is apparent that this type of modulation spectroscopy is quite sensitive to interface conditions, and that it can reveal unexpected variations in materials. The similarity of the spectra for samples from IEC with amorphous and microcrystalline *n*-layers is surprising. In this regard, spectra on samples from BP Solar were less surprising, since the spectra for microcrystalline and amorphous *n*-layers were quite distinct. Nonetheless it surprises us that the

cells with amorphous *n*-layers from BP Solar appear to have quite different spectra than those from IEC and NREL.

The second insight involves the origin of the spectra themselves. The standard model [38] for phosphorus doping in a-Si:H involves nearly equal densities dangling bonds (D centers) and of phosphorus atoms bonded to four silicon (P_4 centers); in this model the centers are uncorrelated with each other, and presumably occur randomly in space. However, the optical absorption predicted for this model contains no sharp features such as exhibited in Fig. 3 [36].

The existence of a sharp absorption line suggests transitions between the ground state and a localized excited state of some center in phosphorus-doped a-Si:H. In our previous work we suggested the possibility that P_4D complexes are responsible for this spectral feature [36], and we describe this model in the next section. Indeed Street [38] has previously noted that formation of such complexes is favored at high doping levels (beyond those used to develop the "standard doping model"). Positron annihilation measurements [39] are also consistent with complexing at high doping levels.

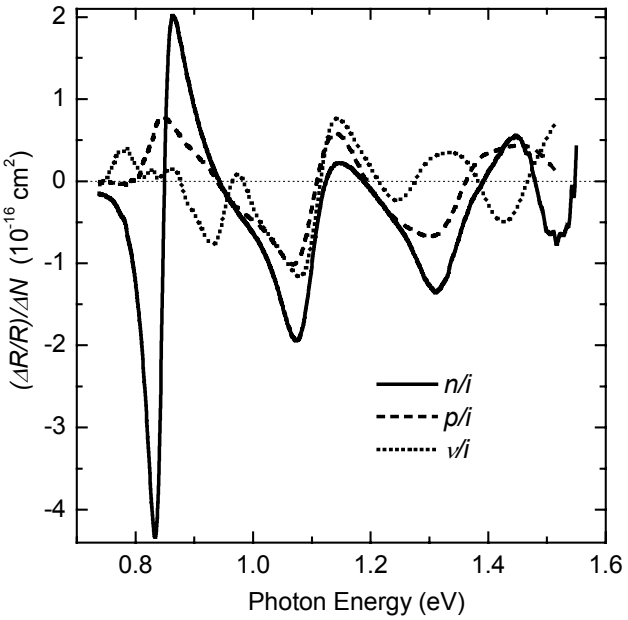

Fig. 14: Reflection modulation $\Delta R/R$ induced by interface charges (areal density ΔN). The key notations *n/i* and *p/i* indicate spectra with light incident through the *n* and *p* layers of the *pin* structure from NREL; the notation *ν/i* indicates spectra with light incident through the *n*-layer of the *piνn* structure from NREL.

Interface Modulation Spectroscopy & Phosphorus-Defect Complexing

Introduction

We recently reported electromodulation spectra measured on diode structures incorporating intrinsic a-Si:H and a variety of *n*-type doped layers [40]. These spectra reveal the well-known electroabsorption spectrum for a-Si:H [41] which peaks near 1.8 eV (essentially the bandgap of a-Si:H). In addition we observed a variety of infrared features in the range 0.7 – 1.2 eV, and in particular a prominent peak at 0.8 eV in several samples. These latter features are most likely due to modulation of the interface charge near the *n/i* interface of the diode structures. As reverse bias is applied and removed to the diodes, charge flows onto and off of these interfaces essentially as if the sample were a simple parallel plate capacitor. We illustrate these essential results and ideas in Fig. 11. The magnitude of the optical cross-section we calculate based on the interface charge modulation model for the spectrum is 10^{-16} cm^2.

The fact that the interface-charge modulation spectrum is a fairly narrow peak surprised us; electronic absorption spectra in a-Si:H usually consist of very broad (several eV) bands with well-defined thresholds. In the present paper we discuss two models for the spectrum. The first model is based on the standard picture for doping in n-type a-Si:H incorporating isolated, fourfold coordinated phosphorus atoms P_4 with levels near the conduction bandedge (or mobility edge). This approach doesn't appear to describe the measurements. We also discuss the spectrum for phosphorus-dangling bond complexes P_4D, which may prove a more satisfactory basis for understanding the measured spectra. In the concluding

section we discuss the possible observation of P_4D in the context of the extensive prior work on doping in *n*-type a-Si:H; a convincing demonstration of a significant role for P_4D would considerably alter our views of interfaces involving *n*-type a-Si:H.

Standard Doping Model

In 1982 R. A. Street proposed a model for incorporation of phosphorus and other doping atoms into a-Si:H which appears to be a quite satisfactory basis for understanding most doping-related phenomena in a-Si:H [42]. We therefore commence by describing predictions based on this model for interface-charge modulation spectra in doped a-Si:H.

An important feature of the model for doping proposed by Street is that it accounts for the observed correlation of electrically active doping with dangling bond creation. In its simplest form, the model calls for creation of equal densities of *charged* P_4^+ and D^- (dangling bond) centers. Although there is a Coulombic energy gained if the centers are generated as intimate pairs during growth, most experiments are better explained by assuming that the centers are uncorrelated in location [42].

We therefore turn to the changes in optical properties associated with occupancy changes for bandtail states (including P_4). We use the viewpoint developed to interpret *photomodulation* spectra by J. Tauc' research group [43]; essentially the same approach was used by Eggert and Paul to interpret electromodulation spectra in a-Si:H based diodes under forward bias [44]. Electrons occuping bandtail levels (either intrinsic or doping-related) should contribute a broad band to optical absorption which starts at the threshold energy E_C-E_F for excitation of an electron to the mobility-edge. As the Fermi energy moves slightly deeper into the bandgap, and away from the bandedge, this contribution to absorption is *bleached*. We have illustrated this effect in Fig. 15. On the left we show the emptying of a bandtail level as the Fermi energy falls; to the right, the dashed line illustrates the onset of a corresponding band of bleached optical absorption (negative values for the optical cross-section σ).

Concurrent with bleaching, this motion of the Fermi energy opens up new states for a band of optical absorption involving valence-band electrons at or below the valence bandedge. The threshold for this *induced* absorption is about E_F-E_V, as illustrated by the longer arrow at the left of Fig. 2. To the right of Fig. 2 we have shown the onset of induced absorption in the continuation of the dashed curve. We have arbitrarily assumed that the induced transition has a somewhat larger optical cross-section than the bleached transition, so the net change in cross-section above the second threshold is positive [45]. At the right of Fig. 15 we also illustrate the prominent feature we measure near 0.8 eV; it is apparent that bleaching and inducing of transitions involving bandtail states is not adequate to explain the measured spectrum.

Since direct optical measurements in phosphorus doped a-Si:H indicate a threshold for the photodetachment of an electron from the D^- level of about 0.9 eV, it is plausible that this transition is somehow involved in the electromodulation spectrum. However, we do not believe that this is the correct model. We first note that depletion of isolated D^- levels in the *n*-layer is negligible, thus ruling out a direct mechanism. The application of reverse-bias to an a-Si:H based diode typically involves an interface charge of the order of 10^{-4} C/m^2, involving about 10^{11} states/cm^2. Only a very small thickness of *n*-type material is involved; at most these charges are spread through 10 nm of the material. The associated band-bending in the n-layer is thus about 0.01 V. Since the Fermi energy itself is at most 0.2 eV below the conduction bandedge in the *n*-type layer, depletion of a level 0.9 eV deep is insignificant. We have been unable to find any other mechanism for a direct influence of the Fermi energy upon the photodetachment spectrum of an isolated D^-.

Doping-Complex Model

At sufficiently high phosphorus incorporation there should be a crossover to doping involving creation of complexes of P_4 and D (denoted P_4D) [42]. We therefore examine possible optical transitions of intimate pairs as a possible origin for our interface-charge modulation spectra.

The optical spectrum associated with such a complex may be surprisingly intricate. In Fig. 16 we illustrate the proposed transitions; the transitions are further identified in Table 1. As regards the optical properties measured in response to Fermi level modulation, there is one main distinction between the properties of the complex and those of the simple bandtail level. This distinction is the presence of an internal excitation of the complex (transition 4) which is not associated with creation of a mobile electron or hole. This transition may account for the sharp, 0.8 eV spectrum we find in several diode samples. As indicated in Fig. 3, the transition is present only in the neutral complex $P_4^+D^-$, so this absorption is induced by depletion of electrons from negatively charged, $P_4^0D^-$ complexes.

We do not expect much effect in electromodulation from transitions 1 and 3; these transitions occur with comparable strength and energy for both of the charge states of the complex. We do predict absorption and bleaching bands (transitions 5 and 2, respectively) similar to those in Fig. 15. However, we have no clear evidence for such features in our observed spectra. This absence may be understood if the optical cross sections for transitions 5 and 2 are about ten times smaller than for transition 4.

We have estimated $\sigma \approx 10^{-16}$ cm^2 for transition 4 by normalizing the relative change in absorption by the number density of interface charges. This magnitude for σ is practically the same magnitude which is estimated for photodetachment of electrons from isolated D^0 and D^- centers [46,47]. We are unaware of direct measurements from which we might infer the optical cross-section for detachment of an electron from an isolated P_4^0, which we might use to infer the cross-section for transitions 5 and 2. We can only speculate as to whether the cross-section might be smaller than those involving D.

Discussion

To date we have explored samples with four different types of *n/i* intefaces. We note that the main feature we have discussed, which is a spectral band centered at about 0.8 eV, is not present for one type

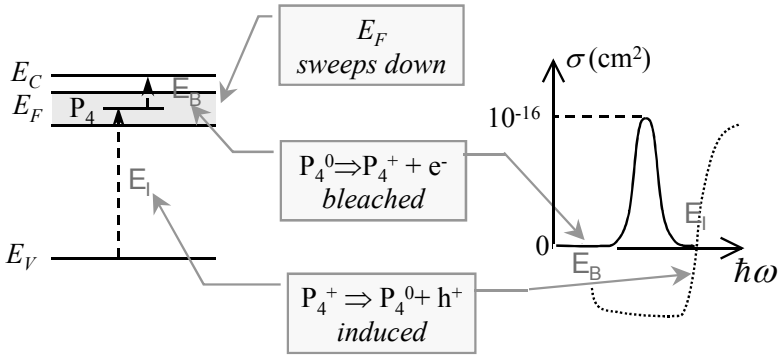

Fig. 15: Optical effects resulting from a change in the Fermi-energy in phosphorus doped a-Si:H. The drawing on the left indicates the depletion of occupied states such as P_4 near the bandedge of a-Si:H as the Fermi energy is lowered. The occupied states contribute a band to optical absorption (threshold about E_C-E_F) which is bleached when the Fermi energy falls. The bleaching band is illustrated to the right of the figure as the dashed line; bleaching accounts for the negative value for the optical cross-section σ. Depletion also opens up a final state for a band of optical transitions originating from the valence band, leading to an induced absorption above a threshold near E_F-E_V as illustrated. The solid line spectrum represents measurements on several samples.

of interface. There are also some weaker, highly variable spectral features which we have also not addressed here.

If we accept the proposed dominance of P_4D complexes in some types of n-type a-Si:H, we should discuss the absence of a significant density of such complexes in previous analyses [42]. The main argument is the following. "Unpaired" D and P_4 centers lead to a prediction that the densities of these centers scale as $[P]^{1/2}$ with the gas-phase phosphorus density during deposition; this prediction is reasonably consistent with published measurements on thin a-Si:H:P films. The electrical efficiency of doping thus *declines* as the phosphorus density increases. If doping were dominated by P_4D complexes, the density should scale as [P]. There is no published evidence of which we are aware supporting this latter scaling.

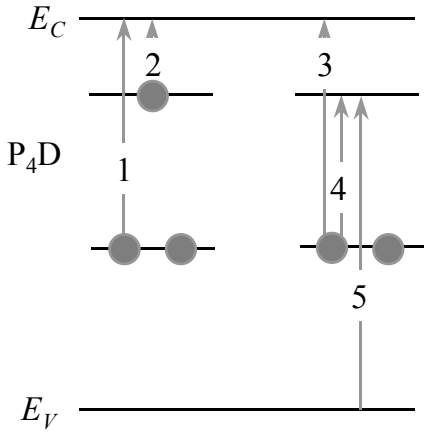

Fig. 16: A P_4D complex has five optical transitions which may contribute to optical effects. We propose that transition 4 in the diagram, which corresponds to an internal excitation of an electron from a deep level to a shallower one, is the origin of the interface-charge modulation spectrum found in infrared electromodulation measurements.

This argument is not (in our view) conclusive in ruling out the presence of P_4D for our particular samples. These all involve very high doping levels which are at the upper limit of the previous studies. Additionally, the present work involves interface regions which arguably may have different properties than thicker films.

The present spectroscopic argument in favor of complexes at *n/i* interfaces thus appears to us to be a plausible speculation requiring further experimental confirmation. We suggest that it would be worthwhile to repeat the earlier thin-film based studies as a function of phosphorus density using *n/i* interfaces. We would anticipate that the contribution of complexes to the interface charge modulation signal should decline with reduced doping density; the absence of the 0.8 eV band in some samples is thus further encouragement for this experiment.

Interface Absorption Spectroscopy under Optical Bias

Introduction

The infrared interface modulation spectrum is actually a superposition of *n/i* and *p/i* interface spectra, and the assignment of a spectral feature to one or the other interface has been done indirectly. In this section we present measurements designed to separate these two contributions more directly by using « optical bias » (auxiliary, visible illumination) and fairly thick samples. The optical bias shifts the position of the positive space charge from its dark position near the *n/i* interface to a position near the middle of the intrinsic layer, so we expect that features from the *n/i* interface are suppressed. The principal result of the present work is the unexpected observation of a spectral line induced by optical bias. By analogy with our previous arguments for *n*-type material, we propose that this line is due to internal transitions of dopant-defect complexes within the *p*-layer. We discuss shifts in the spatial location of the depletion-modulation region as the mechanism for the sizable variations in depletion-modulation spectra for cells from different laboratories and for the optical bias effects.

Experiment details

In this paper we present data from diodes from a single deposition done at BP Solar onto glass coated with textured SnO_2. The *p*-type layer deposited onto the SnO_2 was a-SiC:H:B, followed by a-Si:H and by *n*-type a-Si:H:P. The intrinsic layer was 950 nm thick as inferred from capacitance measurement.

A sinusoidally modulated reverse bias was applied to the sample. A scanning monochrometer (16nm bandpass) was used to probe the sample (probing range from 0.75 eV to above 2.0 eV). The relative, modulated transmittance $\Delta T/T$ was measured using a c-Si pin photodiode in the visible range, and an InGaAs photodiode in the infrared; the modulated photocurrents were recorded using a lockin amplifier. We studied both dark and light biased signals. In light-biased experiments, a laser-diode (685 nm, 20 mW) was used to illuminate the sample. Good care was taken to eliminate stray light from 685 nm laser beam.

Measurements

Fig. 17 shows the relative modulated transmittance spectrum $\Delta T/T$ through the *pin* solar cell for four conditions of electrical and optical bias; a previously published spectrum for an *n/i*/TCO structure [28] is also shown for reference. The principal feature in the dark spectra is the large peak near 1.85 eV; this feature, which depends upon the magnitude of the DC potential V_{DC} across the cell, is the well-known interband electroabsorption of the intrinsic, a-Si:H layer of the cell [48]. The voltage dependence originates in the fact that electroabsorption depends quadratically upon electric field for a-Si:H. The weaker infrared signal is nearly independent of V_{DC} in the dark. The infrared signal is attributed to the change in optical transmission as the charge state of dopants and defects near the interfaces is modified by the sinusoidal modulation of the electric potential across the cell [28]. The figure also illustrates the pronounced differences in the infrared spectra for different structures; the *n/i*/TCO structure (prepared at the Institute of Energy Conversion, University of Delaware) has an obvious spectral feature near 0.8 eV which is absent from the BP Solar specimen. We believe this variability reflects differences in the *n/i* interfaces of the structures, but we aren't yet able to propose a specific mechanism.

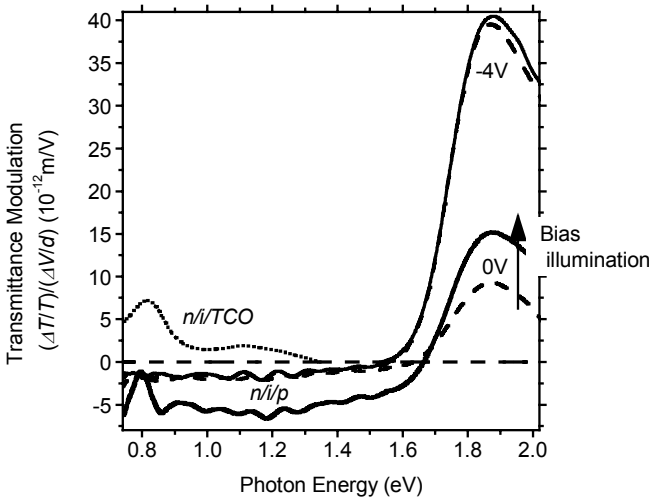

Fig. 17: Normalized transmittance modulation spectrum $d\Delta T/(T\Delta V)$ for an amorphous silicon-based *pin* solar cell prepared at BP Solar (ΔV is the applied modulation voltage, and d is the thickness). A previously reported spectrum [28] for an *n/i/TCO* structure is also shown for reference. Dashed lines are signals measured in the dark. The larger, voltage-dependent peak near 1.85 eV corresponds to *interband electroabsorption*. The weak, voltage-independent *negative* infrared response is due to charging and discharging of dopant and defect levels near the *n/i* and *p/i* interfaces. The solid line spectra are measured under bias illumination (photocurrent 3.4 mA/cm^2); note the line in the 0 V spectrum near 0.8 eV. (Spectra measured at 400 Hz).

As we turned on the bias light, at 0 V there was an

increase in the strength of the visible electroabsorption signal, the broad, negative infrared band strengthened, and a sharp positive feature stands out at 0.8 eV. These effects should be considered in light of the "field-collapse" effect in this type of diode under optical bias; a simulation of this effect is illustrated in Fig. 18, which shows electric field calculated using the AMPS PC-1D computer program [49]. Most parameters used in this simulation were published previously [50], and of course the intrinsic layer thickness was matched to that of the BP Solar cell under discussion. In Fig. 18, solid lines indicate the field distribution under biased light; dashed lines indicate the field distribution in the dark. Two reverse bias voltages (0V/-4V) were used in the simulation.

As we can see in Fig. 18, the field inside the intrinsic layer was uniform through the middle portion of the cell, and increases in magnitude at interfaces. The electric field with 0 V applied is of course the built-in field of the *pin* diode. As we turn on the bias light (uniform illumination), photocharge builds up to some degree in the inside intrinsic layer. Electrons are swept into the electrode layer faster than holes, and this leads to the field collapse inside the intrinsic layer. The field collapse effect becomes much weaker as the reverse bias voltage is increased (in magnitude).

We can use this simulation to help explain the measurements. The increase in interband electroabsorption strength with optical bias is due to the quadratic character of electroabsorption. Roughly speaking, electroabsorption is proportional to the mean-square field in the intrinsic-layer. The applied voltage determines only the mean field: the mean square field, and the electroabsorption signal, increase as the field becomes non-uniform.

In Fig. 19 we have replotted the infrared portion of the electromodulation spectrum on a more sensitive scale. We have normalized the spectra so that they yield the change in optical cross-section due to the change in charge-state. For the optically biased spectra we have further scaled the spectra so that they have the same electroabsorption magnitude in the visible, which roughly compensates for the increase in capacitance of the structures under optical bias.

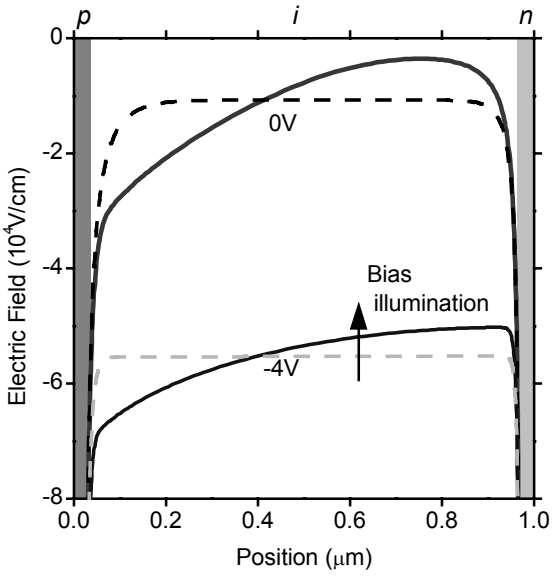

Fig. 18: Electric field profiles in a *pin* solar cell. The data was generated from computer simulations. Two different bias voltages (0V and –4V) were used as in real experiments. Dashed lines are simulation result of field distributions under dark; solid lines indicate field distributions under bias light illumination (uniform photogeneration, 18 mA/cm^2. Significant field-collapse occurs at 0V; very weak field-collapse effect exists at –4V.

Discussion

We see three principal questions associated with these measurements:

1. Why is there so much variability in the dark spectra for cells from different laboratories? In particular, why is the previously observed band near 0.8 eV missing from the BP Solar cells?
2. Why does the broad, negative, infrared spectrum in the BP Solar cells strengthen under optical bias?
3. What is the origin of the sharp line near 0.8 eV under optical bias in the BP Solar cells?

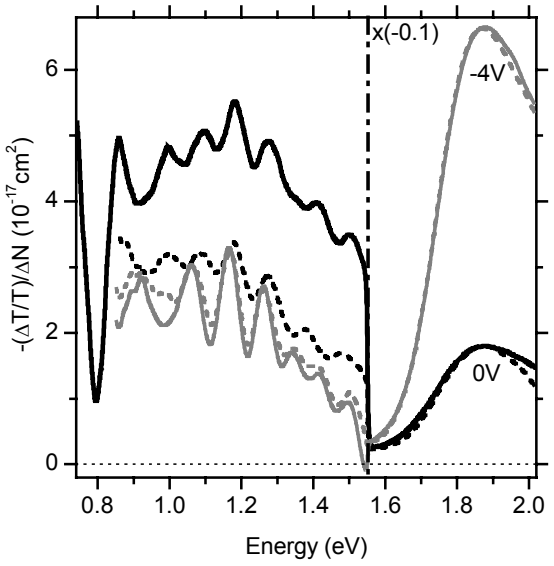

Fig. 19: Transmittance modulation spectrum $\Delta T/T$ for an amorphous silicon-based *pin* solar cell prepared at BP Solar; the modulation has been normalized by the areal density ΔN of charges deduced from simultaneous capacitance measurements. Dashed lines are signals measured in the dark; solid lines indicate signals measured under bias light illumination. Measured with 400 Hz. Photocurrent was 3.4 mA/cm^2, and open-circuit photovoltage was 0.82 V.

We first discuss the fact that the 0.8 eV band seen in the dark for cells from several other sources is missing in the BP Solar cells. We believe that this difference probably indicates that phosphorus dopant-defect complexes are missing from the region near the *n/i* interface in BP Solar cells which is depleted by reverse bias voltage; one model would be that this region lies within the intrinsic layer in the BP Solar cells, and extends into the n-layer in the cells with a 0.8 eV band.

We next discuss the broad, negative infrared spectrum in the BP Solar cells. Such broad spectra are fairly well known from photomodulation spectroscopy in doped and undoped a-Si:H [51], and indeed it is the sharp lines seen in depletion modulation spectra which are most surprising. Depletion of defect and dopant levels near the *n/i* and *p/i* interfaces reduces the direct optical ionization cross-section from these states, and accounts for a negative sign over at least some part of the spectral range. A more detailed discussion can be carried out using analysis developed for photomodulation [36,51]. Under optical bias, we believe that electron depletion shifts from locations near the *n/i* interface to locations within the intrinsic layer, so physically distinct levels are being depleted, presumably with somewhat different optical properties than those at the *n/i* interface.

Finally, we consider the sharp, 0.8 eV feature under optical bias. As just discussed, we exclude the *n/i* interface for these effects. Sharp infrared spectra have never been reported for intrinsic a-Si:H in direct absorption, photomodulation [51], or injection modulation [52] spectroscopies. We therefore assign this feature to the *p*-layer (a-SiC:H:B) of these cells. We also again assign the spectrum to internal optical transitions of a boron dopant-defect complex (presumably B_4D); we are aware of no other mechanism for explaining a sharp spectral feature due to electronic transitions in amorphous semiconductors. The coincidence of this line's position with that previously ascribed to phosphorus-doped a-Si:H [36] is surprising. Even more unexpected was that this line appeared only under optical bias, and was absent in the dark. We speculate that this effect is due to a shift of the depletion modulation region from within the intrinsic material (in the dark) to a region with the *p*-layer (under illumination).

Hydrogen-mediated models for metastability in a-Si:H: Role of Dihydride bonding

Introduction

Practically since its discovery over 25 years ago, scientists have known that the electronic properties of hydrogenated amorphous silicon (a-Si:H) not only vary greatly from sample to sample, according to deposition conditions, but that a given sample will exhibit metastable behavior according to its history of illumination or thermal treatment. Since bonded hydrogen is clearly essential to these electronic properties, it is plausible that differing bonding arrangements may explain both types of variability. Nonetheless a comprehensive model relating hydrogen and electronic properties has never emerged.

There have been significant successes in hydrogen-mediated models for specific phenomena. In 1988 Jackson and Kakalios [53] showed that thermal annealing times for a metastable conductivity were reasonably consistent with hydrogen-diffusion measurements. In 1989, Zafar and Schiff [54] showed that the clustered phase of hydrogen revealed by nuclear magnetic resonance measurements could be used to explain how the density of dangling bonds increased as hydrogen was removed from a-Si:H in evolution experiments. Quite recently, Branz showed how the kinetics of light-induced defect generation can be explained by hydrogen collisions [55] and Biswas proposed an entirely new class of hydrogen-mediated models to account for metastabilities in optical and structural measurements [56].

Here we present a proposal for marrying the hydrogen-mediated models proposed by Zafar and Schiff and by Branz. The crucial feature of both models is their assumption that hydrogen pairs can be more stable than isolated hydrogen on certain sites; the concept is reminiscent of "negative electronic correlation energies." In both models, dangling bonds are generated by transferring two hydrogen atoms bonded at isolated sites onto a single pair-site; there is thus only a single type of dangling bond which is not intimate with hydrogen. Despite the strong common feature, the models differ in a crucial detail: in equilibrium, pair-sites are mostly filled with hydrogen in the clustered-phase model, but are mostly empty in the hydrogen-collision model.

We propose here that clustered phase sites can bond two pairs of hydrogen. Under most conditions, these sites are occupied by only a single pair. When occupied by two pairs, we identify the sites with "dihydride-bonded hydrogen" often measured in a-Si:H [57]. The model predicts that annealing times for light-induced defects in "dihydride poor" a-Si:H be comparable to annealing times for thermally quenched defects in "dihydride-rich" a-Si:H; recent measurements by Quicker and Kakalios [57] appear to be consistent with this prediction.

Clustered-Phase Model

NMR measurements reveal the existence of 2 distinct environments for hydrogen in a-Si:H: "dilute-phase" hydrogen, which most likely converts to a simple dangling bond when its hydrogen is removed, and "clustered-phase" hydrogen, whose exact structure remains obscure. Zafar and Schiff [54,58] proposed the hydrogen level diagram shown in Fig. 20 (left) to account for several properties of the dangling bond density. The single level associated with the clustered-phase is actually the average of level positions for the two hydrogen atoms bound at a clustered-phase site; the original paper [54] should be consulted for a more complete description of the statistical mechanics of such pair-levels. The hydrogen chemical potential μ_H is set somewhat above the clustered-phase level, so that most of the sites in both phases are occupied by hydrogen. This level diagram accounts quite accurately for measurements of the temperature-dependent dangling bond density, of the dangling bond density as hydrogen is evolved from a sample [53], and of the annealing times for metastable dangling bonds created by thermal

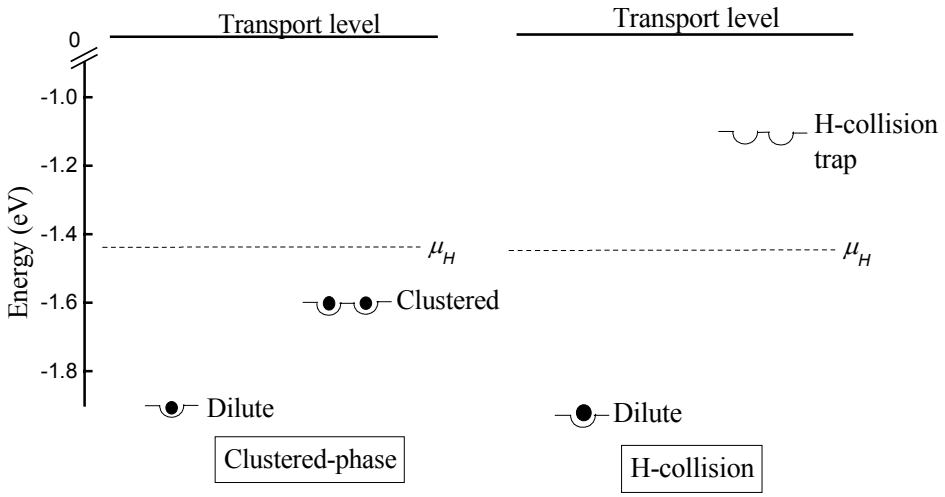

Fig. 20: Hydrogen level diagrams for the clustered-phase and hydrogen-collision models. Note that levels corresponding to both the clustered-phase and to the collision pair-trap are pair levels, implying a slight modification of ordinary one-particle statistical mechanics. The level position for the clustered phase was set to correspond to annealing measurements for thermally quenched spins; the dilute-phase level was set 0.3eV lower to account for the temperature-dependent spin density. The chemical potential is set to account for typical spin densities at 200C. For the H-collision model, the level for the pair trap was set from Staebler-Wronski annealing measurements; the dilute-phase level and the chemical potential were set the same as for the clustered-phase model. Absolute values of the level positions are set assuming that hydrogen motion is not thermally activated in the transport level

quenching [59,60]. We have reproduced these annealing-time measurements from the literature in Fig. 21, along with annealing times from several other experiments which we discuss subsequently.

Hydrogen-collision Model

The hydrogen-collision model developed by Branz [55] accounts for several experiments probing the transient dangling bond density during illumination. In Fig. 20 (right), we present a level diagram which we believe is consistent with the hydrogen-collision model. The main change *vis a vis* the clustered-phase model is a raising of the pair-level above the chemical potential μ_H. The raising permits the H-collision model to account for two important aspects of light-induced dangling bonds. First, the activation energy for annealing of light-induced dangling bonds is significantly smaller than the activation energy for annealing of metastable dangling bonds created by thermal quenching. The experimental data on annealing times for quenched [59,60] and for light-induced [61,1,62] defects is presented in Fig. 21. The pair levels positions below the H-transport level in Fig. 20 were set to correspond with the activation energies in Fig. 21 (1.6 eV for quenched dangling bonds, 1.1 eV for light-induced) [63].

The second aspect requiring a pair level above μ_H is light-induced annealing, which is invoked to account for the steady-state dangling bond density reached after long illumination. In the hydrogen-collison model, light-induced detrapping of H-pairs is negligible in equilibrium, but rises proportional to the density of hydrogen trapped in pair-sites. Ultimately a balance is reached by light-induced H-generation from dilute phase sites, and light-induced detrapping from pairs. These properties require that the initial density of H on the pair-level be much less than the density of empty-sites for the dilute level (ie. much less than the initial dangling bond density). Correspondingly, the chemical potential must satisfy:

$$(\mu_H - E_D) < 2(E_P - \mu_H) \quad (1)$$

where E_D and E_P denote the dilute and pair level positions, respectively. μ_H is evaluated at about 200 C, since room-temperature spin densities are quenched in around 200 C. We have assumed that the densities of dilute-phase and pair-trap levels are equal. The factor 2 emerges from the properties of pair levels. It is noteworthy that the level positions in Fig. 20, which were chosen to match several activation-energy experiments, satisfy this constraint without adjustment.

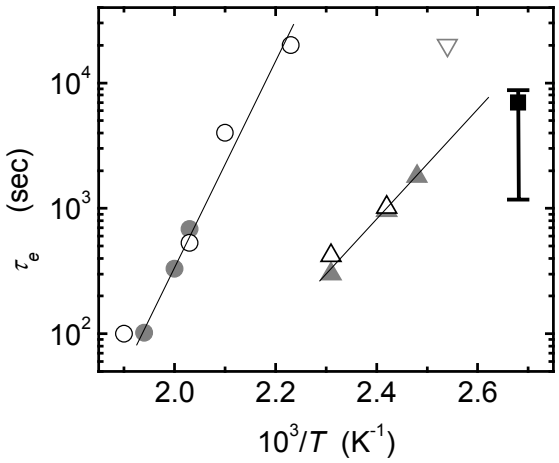

Fig. 21: Annealing times for quenched defects (circles) and for light-induced defects (triangles). The data points were taken from the literature: solid circles [59], open circles [60], solid triangles [53], open up-triangles [61], open down-triangle [62]. Annealing time for dihydride-rich material is shown as a square with a corresponding error bar. This data point was taken from ref [57]. The lines present thermally activated process with activation energy 1.6 eV for quenched and 1.1 eV for light-induced defects.

The Dihydride Model

It is essential to marry these two models to have any claim to a comprehensive view of dangling bonds and hydrogen in a-Si:H. We propose the level diagram presented in Fig. 22. The key assumption is that clustered-phase sites can now bind either one or two hydrogen-pairs. The marriage is fairly uncomplicated: the thermal equilibrium properties are largely controlled by the lower pair level, whereas non-equilibrium properties such as the Staebler-Wronski effect can be dominated by the upper level.

Since this newly proposed model mainly joins less comprehensive models for defects and hydrogen, it largely inherits their desirable properties without predicting much which is new. However, we furthermore propose that dihydride bonding, which is frequently observed in a-Si:H, corresponds to the upper pair level of a clustered-phase site. We have illustrated the identification of levels with bonding configurations in Fig. 22.

This dihydride-bonding proposal admits at least one new experimental test. In Fig. 21, we compare annealing times for dangling bonds in dihydride-rich material with annealing times for light-induced spins in conventional a-Si:H, which has little dihydride-bonding. Although there is precious little published data on equilibration times in dihydride rich material, the one datum does appear similar to the annealing times for light-induced defects in normal a-Si:H. While certainly not a conclusive test, this coincidence, which has not to our knowledge been noticed before, indicates that a more thorough examination of the "dihydride" model may be fruitful.

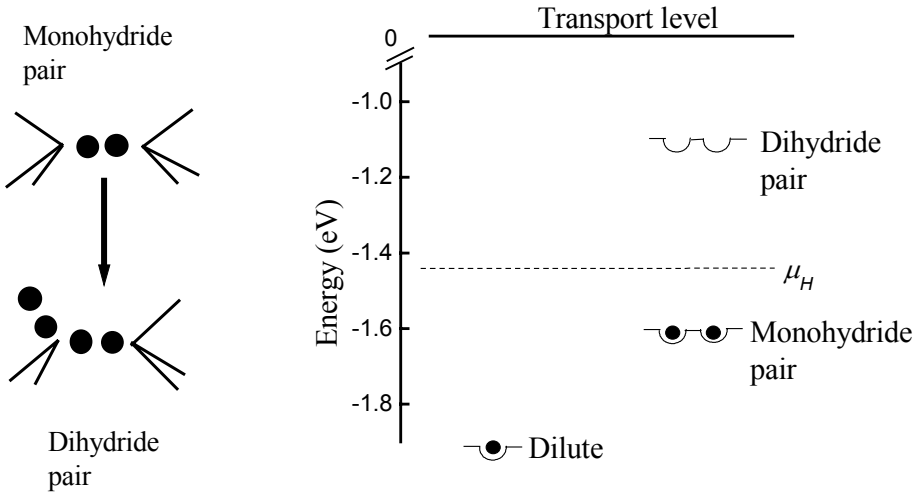

Fig. 22: Hydrogen level diagram and bonding configurations for the dihydride model. Note that monohydride and dihydride states are pair levels.

Polymer-Amorphous Silicon Heterojunction Devices

Introduction

Organic and polymeric electronic materials have been increasingly used in recent years in light-emitting diodes and other devices [64]. The wide range of optical and electronic properties of organic semiconductors indicates that incorporation of these materials into electronic devices in combination with inorganic semiconductor may result in better performance than for devices fabricated exclusively with inorganic (or organic) semiconductors. In fact, there have been several recent reports on such organic/inorganic hybrid devices, in particular for thiophene derivative polymers on crystalline Si [65] CdS [66], and GaAs [67]. In this paper we report our results on fabrication of hydrogenated amorphous silicon (a-Si:H) thin film solar cells with a hole-conducting polymer as the window layer.

The polymeric semiconductor could be a replacement in future for the inorganic p-layers in amorphous silicon solar cells. In present technology, boron-doped, hydrogenated amorphous silicon-carbide [68] (a-SiC:H:B) or boron-doped, hydrogenated microcrystalline silicon [69] (μc-Si:H:B) thin film is used as a window layer. The device parameter most affected by the *p*-layer is the open-circuit voltage, which is in the range 0.90-0.95 V (solar illumination) for devices with hydrogen diluted intrinsic amorphous silicon layers. We have been exploring polymer hole-conductors as a window layer of a-Si-based solar cells because they can have larger bandgaps and simultaneously higher conductivity than the present inorganic p-layers, which may lead to improvements in either the optical performance (by reduction in the window layer absorption) or electrical performance (by increase of the built-in potential or of the conduction band offset at the *p/i* interface [70]). In the present work, we obtained open-circuit voltages up to 0.72 V, which demonstrates that polymer hole conductors work as *p*-layers in amorphous silicon-based solar cells.

Experimental Details

We selected the hole-conducting polymer blend PEDOT;PSS[1] [71], which has satisfactory transparency in the visible region of solar spectrum as well as high conductivity (up to 30 S/cm). The *n*-type (phosphorus doped) and intrinsic a-Si:H films were deposited on stainless steel substrates using hot-wire chemical vapor deposition; the *n*-type layer was about 30 nm thick, and the intrinsic layer was 500 nm thick. For some devices, the top surface of the intrinsic a-Si:H film was etched using hydrofluoric acid before applying the aqueous solution of PEDOT:PSS, and in some other devices, the polymer solution has been directly applied on unetched a-Si:H film. The polymer solution was applied either by painting or spin-coating. The structures were then annealed at atmospheric pressure at 110°C for one hour to cure the polymer layer. Both surface treatment of the a-Si:H layer and subsequent annealing of the polymer affect the properties of the diode.

Results

Fig. 23 shows dark and light current-voltage (*J-V)* characteristics of a-Si:H solar cells with PEDOT:PSS as the window layer; these diodes were fabricated without acid etching of amorphous silicon layer before the polymer was put down. The "X" symbols represent the dark *J-V* characteristic of one such diode . It can be seen in Fig. 1 that current starts leaking for reverse bias voltages exceeding –1 V; the rectification ratio of the currents at +1 and –1 V is ~10. This breakdown under reverse bias is much reduced if the polymer layer is fabricated by the spin-casting method, for which a rectification ratio as high as 10^3 has been obtained. However, the a-Si:H diodes with spin-cast p-layers actually had somewhat inferior

[1] {poly(3,4-ethylenedioxythiophene):poly(styrenesulfonate)}

photovoltaic properties than the diodes with painted polymer. The light J-V characteristics of diodes with spin-cast polymer will not be discussed further here.

The solids symbols in Fig. 23 represent photocurrent densities J_{ill} under illumination for different devices with polymer as the window layer. The four *J-V* characteristics correspond to four different intensities under white-light (tungsten-halogen bulb) illumination through the polymer layer. For the lowest intensity (near-dark) illumination, the *J-V* characteristic is similar to that of the first device. The magnitude of the current density increases with illumination. The open symbols indicate the photocurrent-density (difference of current density under illumination and in the dark) under maximum intensity (112 mW/cm^2); the photocurrent density saturates at about –0.25 mA/cm^2. This saturation current is about 40 times less than one would expect with a completely transparent *p*-layer.

The open-circuit voltage (V_{OC}) of this second device was about 500 mV for the maximum intensity illumination (112 mW/cm^2); it may be worth noting that V_{OC} depends rather weakly upon illumination intensities. The cell's *J-V* characteristic for bias voltages approaching V_{OC} is different than that of standard photodiode: the photocurrent (open symbols) actually changed sign for bias voltage around V_{OC}. This behavior is in contrast with the simplest photodiode models, for which the photocurrent is independent of applied bias voltage. Although *J-V* characteristics varied substantially for different cells, we found consistency of this qualitative behavior (photocurrent sign reversal at V_{OC}) in all the cells we studied.

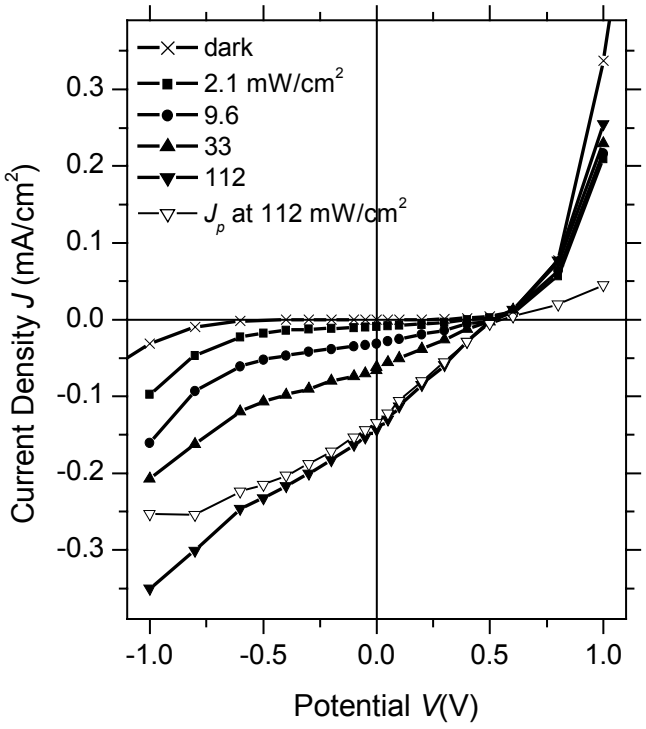

Fig. 23: Dependence of the current density *J* upon applied potential *V* for two a-Si:H:P/a-Si:H/(PEDOT:PSS) heterojunction devices. The X-symbols indicate the dark J-V characteristic of one device; note the pronounced asymmetry, which corresponds to a rectification ratio of dark currents at +1 and –1 V of about 10. Solid symbols indicate the currents for a second, similar device under four different white-light intensities. The open symbols indicate the photocurrent (difference between the current under illumination and in the dark) at the highest intensity (112 mW/cm^2). Note the photocurrent saturation under reverse bias, and the sign reversal in the photocurrent near the open-circuit voltage.

We studied the variation in the open-circuit voltage (V_{OC}) of a-Si:H solar cells with polymer as the window layer for various etching and curing procedures; for these experiments, V_{OC} was measured by a multimeter under outdoor solar illumination. In Fig. 24 we present the variation of V_{OC} with the concentration of hydrofluoric acid (HF) used to etch the surface of a-Si:H (and presumably to remove native oxide); the curve is a Gaussian fit to the data. There is modest improvement in V_{OC} (averaged over numerous

devices) with acid concentration up to a few %; for higher concentrations V_{OC} decreases substantially. The highest V_{OC} obtained so far a-Si:H solar cells is ~ 0.72 V with PEDOT:PSS as the window layer. We do not have quantitative explanations for the observed dependence of V_{oc} vs. HF concentration; however, we do expect that there may be regrowth of the interfacial oxide layer after application of the aqueous solution of PEDOT:PSS.

Discussion

To the best of our knowledge there are no prior reports on polymer/a-Si:H heterostructures with which to compare the present results. The dark and light *J-V* characteristics (Fig. 23) of polymer/a-Si:H solar cells demonstrate that the hole-conducting polymer does act as a *p*-layer in the device. We find dark J-V characteristics are signficantly asymmetric and the photocurrent saturates under reverse bias. These behaviors indicate that the interface between the polymer *p*-layer and a-Si:H injects electrons fairly slowly, and absorbs photogenerated holes without a significant barrier.

There is a pronounced deviation from ideal photodiode behavior for forward bias voltages exceeding about 0.5 V. Under these conditions, the *J-V* characteristic is relatively insensitive to illumination, and indeed the photocurrent itself changes sign near the open-circuit voltage. This behavior for forward bias almost certainly dominates the observed open-circuit voltage of the devices. One speculation for this

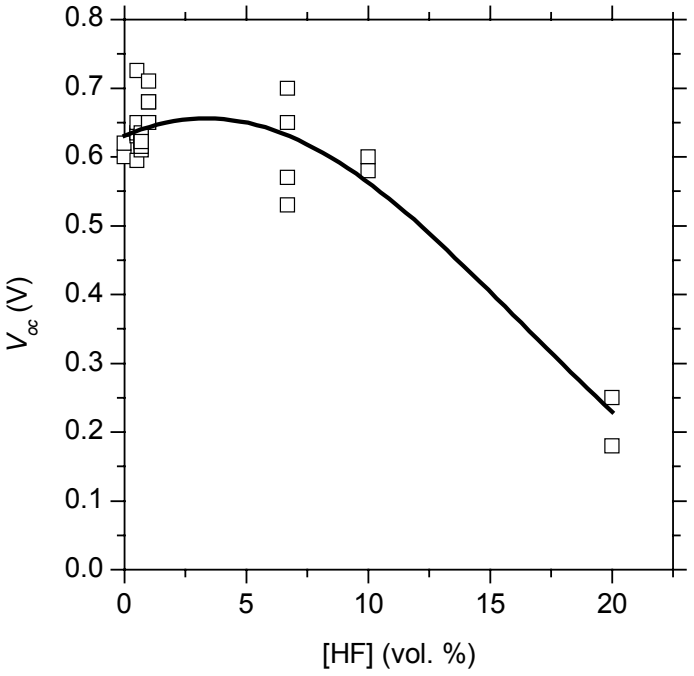

Fig. 24: Open-circuit voltages under AM 1.5 illumination for many a-Si:H:P/a-Si:H/(PEDOT:PSS) solar cells vs. the concentration of HF acid used in etching the a-Si:H surface. The cells were immersed in the acid for 1 minute and then washed in deionized water and dried, after which the polymer was immediately applied. Cells indicated with an acid concentration of0 were unetched prior to application of the polymer. Cells were then heated for 1 hour at 110°C to cure the PEDOT:PSS polymer.

behavior would be that the built-in potential (V_{bi}) across the cells is ~0.6-0.7 V. The mean electric field – and hence the photocurrent – would then reverse sign for larger electric potentials. The relatively low open circuit voltage (~0.72 V) of a-Si:H solar cells with polymer as the window layer compared to Si-based p-layer can be partly attributed to the low bandgap (~ 1.6 eV) of PEDOT:PSS.

If V_{bi} of polymer/a-Si:H solar cells is indeed ~ 0.7 V, it is 0.5 V lower than electroabsorption estimates (~ 1.2 V) with conventional *p*-layers,72 suggesting that either a very different *p/i* interface, or a polymer with higher bandgap (than that of PEDOT:PSS), will be required to improve upon current devices incorporating silicon-based *p*-layers. PEDOT:PSS is one of the large-class of hole conducting polymers, and it seems likely to us that a-Si:H solar cells with p-type semiconducting polymers having higher bandgaps and conductivities will yield superior photovoltaic properties.

References

1 Lin Jiang, Qi Wang, E. A. Schiff, S. Guha, J. Yang, X. Deng, *Appl. Phys. Lett.* **69**, 3063 (1996).

2 C. R. Wronski, unpublished.

3 S. Nonomura, H. Okamoto, and Y. Hamakawa, Appl. Phys. A 32, 31 (1983).

4 A. Nuruddin and J. R. Abelson, *Appl. Phys. Lett.* **71**, 2797 (1997).

5. H. Zhu and S. J. Fonash, collected in *Amorphous and Microcrystalline Silicon Technology - 1998*, edited by R. Schropp, *et al.* (Materials Research Society, Symposium Proceedings Volume 507, Pittsburgh, 1998), 395.

6. A. Rose, *Photoconductivity and Allied Topics* (Wiley, 1963, New York; reprinted Krieger, 1978).

7. S. J. Fonash, *Solar Cell Device Physics* (Academic, New York, 1981).

8. Despite the fact that this result is well-known, we are unaware of any conclusive proof which would indicate its limitations.

9. S. Wagner, X. Xu, X. R. Li, D. S. Shen, M. Isomura, M. Bennett, A. E. Delahoy, X. Li, J. K. Arch, J.-L. Nicque, and S. J. Fonash, in *Conference Record of the IEEE Photovoltaic Specialists Conference* (Institute of Electrical and Electronics Engineers, New York, 1991), 1307.

10. F. Wang and R. Schwarz, *J. Appl. Phys.* **71**, 791 (1992).

11. T. Tiedje, *Appl. Phys. Lett.* **40**, 627 (1982). A calculator based on Tiedje's expressions is currently available at the web-site http://physics.syr.edu/~schiff/AMPS.

12. L. Jiang, E. A. Schiff, Q. Wang, S. Guha, and J. Yang, *Appl. Phys. Lett.***69**, 3063 (1996).

13. S. Guha, J. Yang, P. Nath, and M. Hack, *Appl. Phys. Lett.* **49**, 218 (1986).

14. Q. Wang, E. Iwaniczko, Y. Xu, W. Gao, B. Nelson, H. Mahan, R. S. Crandall, H. M. Branz, *this volume*.

15. H. M. Branz and R. S. Crandall, *Solar Cells* **27**, 159 (1989).

16. I.-S. Chen and C. R. Wronski, J. Non-Cryst. Solids 190, 58 (1995).

17. W. B. Jackson, S. M. Kelso, C. C. Tsai, J. W. Allen, and S.-J. Oh, *Phys. Rev. B* **31**, 5187 (1985).

18. E. A. Schiff, R. I. Devlen, H. T. Grahn, J. Tauc, and S. Guha, *Appl. Phys. Lett.* **54**, 1911 (1989).

19. G. Juska, K. Arlauskas, J. Kocka, M. Hoheisel, and P. Chabloz, *Phys. Rev. Lett.* **75**, 2984 (1995).

20. Q. Wang, H. Antoniadis, E. A. Schiff, and S. Guha, *Phys. Rev. B* **47**, 9435(1993).

21. E. A. Schiff, *J. Non-Cryst. Solids* **190**, 1 (1995).

22. Q. Gu, Q. Wang, E. A. Schiff, Y.-M. Y.-M., and C. T. Malone,*J. Appl. Phys.* **76**, 2314 (1994).

23. G. Juska, J. Kocka, M. Viliunas, and K. Arlauskas, *J. Non-Cryst. Solids* **164-166**, 579 (1993).

24. P. Stradins, H. Fritzsche, P. Tzanetakis, and N. Kopidakis, in *Amorphous Silicon Technology - 1996*, edited by M. Hack, *et al* (Materials Research Society Symposium Proceedings Vol. 420, Pittsburgh, 1996), p. 729.

25 S. Guha, J. Yang, D. L. Williamson, Y. Lubianiker, J. D. Cohen, and A. H. Mahan, *Appl. Phys. Lett.* **74**, 1860 (1999).

26 E. A. Schiff, Q. Gu, L. Jiang, J. Lyou, I. Nurdjaja, and P. Rao, *Research on High-Bandgap Materials and Amorphous Silicon-Based Solar Cells: Final Technical Report* (NREL document SR-520-25922, 1998), p. 31.

27 Q. Gu, Q. Wang, E. A. Schiff, Y.-M. Li, and C. T. Malone, *J. Appl. Phys.* **76**, 2310 (1994).

28 J. H. Lyou, E. A. Schiff, S. S. Hegedus, S. Guha, and J. Yang, in *Amorphous and Heterogeneous Silicon Thin Films: Fundamentals to Devices – 1999*, edited by H. M. Branz, R. W. Collins, H. Okamoto, S. Guha, and R. Schropp (Materials Research Society, Symposium Proceedings Vol. 557, 1999), 457.

29 J. Lyou, N. Kopidakis, E. A. Schiff, *J. Non-Cryst. Solids* **266-269**, 227 (2000).

30 K. Zhu, J. H. Lyou, E. A. Schiff, R. S. Crandall, G. Ganguly, and S. S. Hegedus, Kai Zhu, J. H. Lyou, E. A. Schiff, R. S. Crandall, G. Ganguly, S. S. Hegedus, in *Conference Record of the 28th IEEE Photovoltaics Specialists Conference* (Institute of Electrical and Electronics Engineers, Inc., Piscataway, 2000) 725.

31 J. Koh, A. S. Ferlauto, P. I. Rovira, C. R. Wronski, and R. W. Collins, *Appl. Phys. Lett.* **75**, 2286 (1999).

32 M. F. Plass, J. Ristein, L. Ley, *J. Non-Cryst. Solids* **164-166**, 829 (1993).

33 I.-S. Chen and C. R. Wronski, *J. Non-Cryst. Solids* **190**, 58 (1995); X. Xu, J. Yang, A. Banerjee, S. Guha, K. Vasanth, and S. Wagner, *Appl. Phys. Lett.* **67**, 2323 (1995).

34 C. Palsule, U. Paschen, and J. D. Cohen, J. Yang and S. Guha, *Appl. Phys. Lett.* **70**, 499 (1997).

35 J. H. Lyou, E. A. Schiff, S. S. Hegedus, S. Guha, and J. Yang, in *Amorphous and Heterogeneous Silicon Thin Films: Fundamentals to Devices – 1999*, edited by H. M. Branz, R. W. Collins, H. Okamoto, S. Guha, and R. Schropp (Materials Research Society, Symposium Proceedings Vol. 557, 1999), 457.

36 J. Lyou, N. Kopidakis, E. A. Schiff, *J. Non-Cryst. Solids* **266-269**, 227 (2000).

37 G. Weiser, U. Dersch, and P. Thomas, *Phil. Mag. B* **57**, 721 (1988).

38 R. A. Street, *Hydrogenated Amorphous Silicon* (Cambridge University Press, Cambridge, 1991).

39 M. P. Petkov, M. H. Weber, K. G. Lynn, R. S. Crandall, V. J. Ghosh, *Phys. Rev. Lett.* **82**, 3819 (1999).

40 J. Lyou, E. A. Schiff, S. S. Hegedus, S. Guha, and J. Yang, in *Amorphous and Heterogeneous Silicon Thin Films: Fundamentals to Devices (1999)*, edited by H. M. Branz, R.W. Collins, H. Okamoto, S. Guha, R. Schropp (Materials Research Society, Symposium Proceedings Vol. 557, Pittsburgh), *in press.*

41 G. Weiser, U. Dersch, and P. Thomas, *Phil. Mag. B* **57**, 721 (1988).

42 R. A. Street, *Hydrogenated Amorphous Silicon* (Cambridge University Press, Cambridge, 1991).

43 Z. Vardeny and J. Tauc, *Phys. Rev. Lett.* **54**, 1844 (1985).

44 J. R. Eggert and .W. Paul, *Phys. Rev. B* **35**, 7993 (1987).

45 W. B. Jackson, S. M. Kelso, C. C. Tsai, J. W. Allen, and S.-J. Oh, *Phys. Rev. B* **31**, 5187 (1985) discuss the "random phase" conjecture that the matrix elements for all of these optical transitions are the same.

46 A. V. Gelatos, J. D. Cohen, and J. P. Harbison, J. Non-Cryst. Solids **77&78**, 291 (1985).

47 W. B. Jackson and N. M. Amer, *Phys. Rev. B* **25**, 5559 (1982).

48 G. Weiser, U.Dersch, and P. Thomas, Philos. Mag. B 57 (1988) 721.

49 H. Zhu and S. J. Fonash, Mater. Res, Soc. Symp. Proc. V507, 1998, 395.

50 L. Jiang, J. H. Lyou, S. Rane, E.A. Schiff, Q. Wang, Q. Yuan, *Amorphous and Heterogeneous Films*, edited by H.M. Branz, R.W. Collins, S. Guha, H. Okamoto, M. Stutzmann (Materials Research Society, Symposium Proceedings, vol. 609, Pittsburgh, 2001), A18.3.1.

51 Z. Vardeny, T. X. Zhou, H. A. Stoddart and J. Tauc, *Solid State Commun.* **65**, 1049 (1988).

52 J. R. Eggert, W. Paul, *Phys. Rev. B* **35**, 7993 (1987).

53. W.B. Jackson and J.Kakalios, *Phys. Rev. B* 37 (1988) 1020.

54. S. Zafar and E. A. Schiff, *Phys. Rev. B* 40 (1989) 5235.

55. H. Branz, *Sol. State Commun.* 105/6 (1998) 387, H. Branz, *Phys. Rev. B* 59 (1999) 5498.

56 R. Biswas and Y.-P. Li, *Phys. Rev. Lett,* 82 (1999) 2512

57. Quicker and J. Kakalios, *Phys. Rev. B*. 60 (1999) 2449.

58. S. Zafar and E. A. Schiff, *Phys. Rev. Lett,*.66 (1991) 1493

59. S. Zafar and E. A. Schiff, *J. Non-Cryst. Solids* 137&138 (1991)

60. X. Xu, H. Sasaki, A. Morimoto, M. Kumeda, T. Shimitzu, *Phys. Rev. B* 41 (1990) 10049.

61. M. Stutzmann, W. B. Jackson, and C.-C. Tsai, *Phys. Rev. B* 32 (1985) 23.

62. Q. Zhang, H. Takashima, J-H. Zhou, M. Kumeda, T. Shimitzu, *Mat. Res. Soc. Symp. Proc.* 336 (1994) 269.

63. An interesting property of pair levels is that their positions, and not that of μ_H, determine measured activation energies.

64 R. H. Friend, R. W. Gymer, A. B. Holmes, J. H. Burroughes, R. N. Marks, C. Taliani, D. D. C. Bradley, D. A. Dos Santos, J. L. Bredas, M. Loegdlund, and W. R. Salaneck, *Nature* **397,** 121 (1999).

65 K. Hoshino, T. Ogata and H. Kokado, *Jpn. J. Appl. Phys.* **34,** L1241 (1995).

66 H. N. Cong, M. Dieng, C. Sene, P. Chartier, *Solar Energy Materials & Solar Cells* **63**, 23 (2000).

67 F. Garnier, unpublished.

68 R. R. Arya, A. Catalano, and R. S. Oswald, *Appl. Phys. Lett.* **49**, 1089 (1986).

69 S. Guha, J. Yang, P. Nath, M. Hack, *Appl. Phys. Lett.* **49**, 218 (1986).

70 L. Jiang, J. H. Lyou, S. Rane, E. A. Schiff, Q. Wang and Q. Yuan, in *Amorphous and Heterogeneous Films – 2000*, edited by H. M. Branz, R. W. Collins, S. Guha, H. Okamoto, and M. Stutzmann (Materials Research Society, Symposium Proceedings Vol. 609, Pittsburgh, 2001), pp. A18.3.1-12.

71 L. Groenendaal, F. Jonas, D. Freitag, H. Pielartzik, and J. R. Reynolds, *Advanced Materials* **12**, 49 (2000). We used the commercial material "Baytron P" available from Bayer Corporation, which consists of 0.5% (weight) PEDOT and 0.8 % (weight) PSS in water.

72 J. Lyou, E. A. Schiff, S. Guha, and J. Yang, *Appl. Phys. Lett.* **78**, 1924-1926 (2001).

REPORT DOCUMENTATION PAGE

Form Approved
OMB NO. 0704-0188

1. AGENCY USE ONLY (Leave blank)	2. REPORT DATE	3. REPORT TYPE AND DATES COVERED
	December, 2002	Subcontract Report

4. TITLE AND SUBTITLE
Electroabsorption and Transport Measurements and Modeling Research in Amorphous Silicon Based Solar Cells: Final Technical Report, 24 March 1998–15 August 2002

5. FUNDING NUMBERS
CF: XAK-8-17619-23
PVP35001

6. AUTHOR(S)
E.A. Schiff, A.R. Middya, J. Lyou, N. Kopidakis, S. Rane, P. Rao, Q. Yuan, and K. Zhu

7. PERFORMING ORGANIZATION NAME(S) AND ADDRESS(ES)
Syracuse University
Syracuse, New York 13244-1130

8. PERFORMING ORGANIZATION REPORT NUMBER

9. SPONSORING/MONITORING AGENCY NAME(S) AND ADDRESS(ES)
National Renewable Energy Laboratory
1617 Cole Blvd.
Golden, CO 80401-3393

10. SPONSORING/MONITORING AGENCY REPORT NUMBER
NREL/SR-520-33164

11. SUPPLEMENTARY NOTES
NREL Technical Monitor: B. von Roedern

12a. DISTRIBUTION/AVAILABILITY STATEMENT
National Technical Information Service
U.S. Department of Commerce
5285 Port Royal Road
Springfield, VA 22161

12b. DISTRIBUTION CODE

13. ABSTRACT *(Maximum 200 words)* The contributions of this research project to amorphous silicon solar cells are in the following areas:

- *Improved understanding of the open-circuit voltage*. We have developed a “thermionic emission model” that explains how defective interfaces in a-Si:H *pin* cells cause diminished values of V_{OC}.
- *Improved knowledge of the built-in potential.* Our estimates of V_{BI} are about 1.2 V in a-SiGe cells. V_{BI} is crucial to understanding the performance of a-Si:H solar cells.
- *Variations in hole drift-mobilities for differing forms of a-Si:H*. We found that both hot-wire-deposited a-Si:H and also hydrogen dilution during plasma deposition yield larger hole drift-mobilities.
- *Infrared spectroscopy of interfaces in a-Si:H cells.* We discovered a method that yields the spectrum of the *p/i* and *n/i* interfaces in a-Si:H solar cells. We made progress in understanding these spectra, although much remains to be done.
- *Polymer p-layers*. We explored a hole-conducting polymer (PEDT:PSS) as the *p*-layer in a-Si:H *pin* cells; the open-circuit voltage is about 0.7 V.
- *Hydrogen-based models for defects and metastability*. We showed how previous work on hydrogen and defects in a-Si:H relates to the more recent “hydrogen collision” model for the Staebler-Wronski effect.

14. SUBJECT TERMS: PV; amorphous silicon; solar cells; open-circuit voltage; drift-mobilities; hot-wire; infrared spectroscopy; polymer p-layers; hydrogen; electroabsorption; transport measurements; modeling; metastability; built-in potential; Staebler-Wronski effect

15. NUMBER OF PAGES

16. PRICE CODE

17. SECURITY CLASSIFICATION OF REPORT	18. SECURITY CLASSIFICATION OF THIS PAGE	19. SECURITY CLASSIFICATION OF ABSTRACT	20. LIMITATION OF ABSTRACT
Unclassified	Unclassified	Unclassified	UL